universität wien

MASTERARBEIT / MASTER'S THESIS

Titel der Masterarbeit / Title of the Master's Thesis

„Developments towards the determination of ^{135}Cs and ^{137}Cs in environmental samples by AMS“

verfasst von / submitted by

Alexander Wieser, BSc BSc

angestrebter akademischer Grad / in partial fulfilment of the requirements for the degree of

Master of Science (MSc)

Wien, 2020 / Vienna, 2020

Studienkennzahl lt. Studienblatt / degree programme code as it appears on the student record sheet:	UA 066 876
Studienrichtung lt. Studienblatt / degree programme as it appears on the student record sheet:	Masterstudium Physik
Betreut von / Supervisor:	Univ.-Prof. Dipl.-Ing. Dr. Robin Golser
Mitbetreut von / Co-Supervisor:	Dipl.-Phys. Dr. Johannes Lachner

Abstract

^{135}Cs has an estimated half-life between 1.3 and 3 Myrs [1]. It is present in the general environment with an isotopic ratio ^{135}Cs/Cs in the order of 10^{-9} or below. The combination of low concentration, low beta end-point energy of 269 keV [2] and long half-life make it specifically hard to determine via radiometric methods [3]. The detection of ^{135}Cs and in particular the isotopic ratio ^{135}Cs/^{137}Cs can be used to assign sources of anthropogenic cesium input, such as global fallout or nuclear accidents like in Chernobyl or in Fukushima [4][5]. ^{135}Cs and ^{137}Cs are decay products of the highly volatile ^{135}Xe and ^{137}Xe, which get produced by nuclear fission and are easily transported into the environment. Due to the high thermal neutron capture cross-section of ^{135}Xe, a "shielding effect" appears for all isobars which are in the decay chain of ^{135}Xe, including ^{135}Cs. Therefore, the fission product ratio of ^{135}Cs/^{137}Cs varies with the number of thermal neutrons emitted in a reactor and can be used as an "isotopic fingerprint".

In classical AMS the separation of interfering isobars is achieved by chemical preparation, selection of suitable negative ions and elemental analysis methods in the detection system. This approach is not possible for cesium detection because ^{135}Ba (6.59 %) and ^{137}Ba (11.23 %) occur at high concentrations in environmental samples such as soils and sediments and are also not distinguishable from cesium by means of stopping power in a gas-filled ionization chamber in typical AMS energy regimes [3]. In this master thesis the method of Ion Laser InterAction Mass Spectrometry (ILIAMS) at the Vienna Environmental Research Accelerator (VERA) was investigated and further improved for cesium detection. This method can utilize differences in the electron affinities of negative ions or molecules [6].

BaF_2^- has a lower electron affinity than CsF_2^- and by overlapping the ion beam with a laser beam of photon energy in between those two electron affinities, the electron of the unwanted isobar gets detached, while the CsF_2^--ions are not affected. The ions get "cooled" in a helium buffer gas filled radiofrequency quadrupole, so that the time for interaction between photons and beam particles lengthens and therefore the suppression gets enhanced. In this master thesis a suppression of more than five orders of magnitudes of these isobars via laser photodetachment was achieved.

In first tests in-house materials but also IAEA reference materials were investigated and results were compared with other groups pursuing different mass spectrometric approaches. The limit of detection was reduced by a factor 100 in this master thesis. The next steps are improving the reproducibility of the samples and minimizing the cross contamination in the ion source, so that eventually environmental samples can be measured at VERA.

Zusammenfassung

^{135}Cs hat eine geschätzte Halbwertszeit von 1.3 bis 3 Millionen Jahren. Es kommt mit einer Häufigkeit von $^{135}Cs/Cs \approx 10^{-9}$ in allgemeinen Umweltproben vor. Die Kombination aus dieser niedrigen Konzentration, einer geringen Betazerfallsenergie von 269 keV und der langen Halbwertszeit machen es schwierig via radiometrischen Methoden zu detektieren. ^{135}Cs, und im speziellen das Isotopenverhältnis $^{135}Cs/^{137}Cs$, kann benützt werden um Quellen eines anthropogenen Cäsiumbeitrags, wie durch Global Fallout oder Nuklearunfälle in Tschernobyl und Fukushima, zuzuordnen. ^{135}Cs und ^{137}Cs sind Zerfallsprodukte der Edelgasnuklide ^{135}Xe und ^{137}Xe, welche leicht in die Umwelt transportiert werden. Durch den hohen Wirkungsquerschnitt zum Einfang thermischer Neutronen von ^{135}Xe tritt ein "Abschirmungseffekt" für alle Isobare in seiner Zerfallskette auf. Dadurch ist das Verhältnis der beiden Spaltprodukte ^{135}Cs und ^{137}Cs abhängig von der Zahl der emittierten Neutronen in einem Reaktor und kann dem zufolge als "Fingerabdruck" der anthropogenen Quelle benützt werden.

In der klassischen Beuschleunigermassenspektrometrie unterdrückt man Isobare durch chemische Präparation, Wahl geeigneter negativer Ionen und elementsensitiver Analyse im Detektorsystem. Für Cs Messungen ist dies aufgrund der hohen Konzentration von Barium in Bodenproben und der Ununterscheidbarkeit der beiden Elemente durch ihr Bremsvermögen in einer gasgefüllten Ionisationskammer in typischen AMS Energiebereichen nicht möglich. In dieser Masterarbeit wurde die Methode der Ion Laser InterAction Mass Spectrometry (ILIAMS) am Vienna Environmental Research Accelerator (VERA) untersucht und weiter verbessert. Diese Methode benützt Unterschiede in den Elektronenaffinitäten der betrachteten negativen Ionen.

BaF_2^- hat eine niedrigere Elektronenaffinität als CsF_2^-. Durch Überlappen des Ionenstrahls mit einem Laserstrahl mit Photonenenergie, welche zwischen den beiden Elektronenaffinitäten liegt, wird ein Elektron des Isobars gelöst, während das zu betrachtende Isotop unbeeinflusst bleibt. Die Ionen werden in einer mit Heliumgas gefüllten Radiofrequenzfalle "gekühlt", um die Zeit der Interferenz zwischen Photonen und Ionen zu verlängern und somit die Unterdrückung des Bariums zu verbessern. In dieser Masterarbeit wurde so eine Unterdrückung von mehr als fünf Größenordnungen erzielt.

In ersten Tests wurden hausinterne Materialien, aber auch IAEA Referenzmaterialien, untersucht und die Ergebnisse mit denen anderer Gruppen mit unterschiedlichen Messansätzen verglichen. Das Detektionslimit konnte um einen Faktor 100 im Rahmen dieser Masterarbeit verbessert werden. Die nächsten Schritte sind die Reproduzierbarkeit der Messung zu verbessern und die Kreuzkontamination in der Ionenquelle zu verringern, sodass schließlich Umweltproben bei VERA gemessen werden können.

Contents

1 Motivation

Cesium is an element with one stable (^{133}Cs), one long- (^{135}Cs) and two medium-lived (^{134,137}Cs) radioactive isotopes. All other isotopes of cesium have half-lives shorter than two weeks. The precursor of cesium in the β^- decay chain is Xenon, a highly volatile noble gas which transports cesium into the environment. ^{137}Cs with a half-life of 30.02 years [7] has important applications, especially after nuclear accidents such as in Chernobyl and Fukushima. ^{137}Cs is quite easily detectable by the 662 keV gamma emission line of its decay product $^{137\mathrm{m}}$Ba. Another cesium isotope of interest is ^{134}Cs. Chino et al. [8] showed that the activity ratio of ^{134}Cs/^{137}Cs can be used to identify the source of contamination and to even assign it to a certain reactor unit of the Fukushima Daiichi Nuclear Power Plant after the accident. ^{134}Cs has a half-life of only 2.06 years [7]. This makes it impractical as a long-term tracer for source identification (fig. 1.1). Also, its decay chain is shielded by the stable ^{134}Xe, so the only relevant way to produce it is over ^{133}Cs neutron capture. Since its independent fission yield is orders of magnitudes lower than for the other relevant radiocesium isotopes, ^{134}Cs is more than one order of magnitude less abundant than its sister isotope ^{137}Cs in the environment right after nuclear accidents.

Another isotope of cesium is ^{135}Cs with an estimated half-life between 1.3 and 3 million years [1]. This isotope is especially interesting as it has a long-enough half-life for long-term measurements but also because of its appearance in the decay chain of ^{135}Xe, which is also known as a "reactor poison". ^{135}Xe has the largest neutron capture cross section of all isotopes and also a medium range half-life of about 9 hours [7]. Therefore there is a strong probability of ^{135}Xe catching a neutron, transforming to stable ^{136}Xe before it can decay further into ^{135}Cs.The transformation rate per unit time is given by

$$\frac{\mathrm{dN}}{\mathrm{dt}} = \phi_{\mathrm{th}} \cdot \sigma(\mathrm{n}, \gamma) \cdot \mathrm{N} \tag{1.1}$$

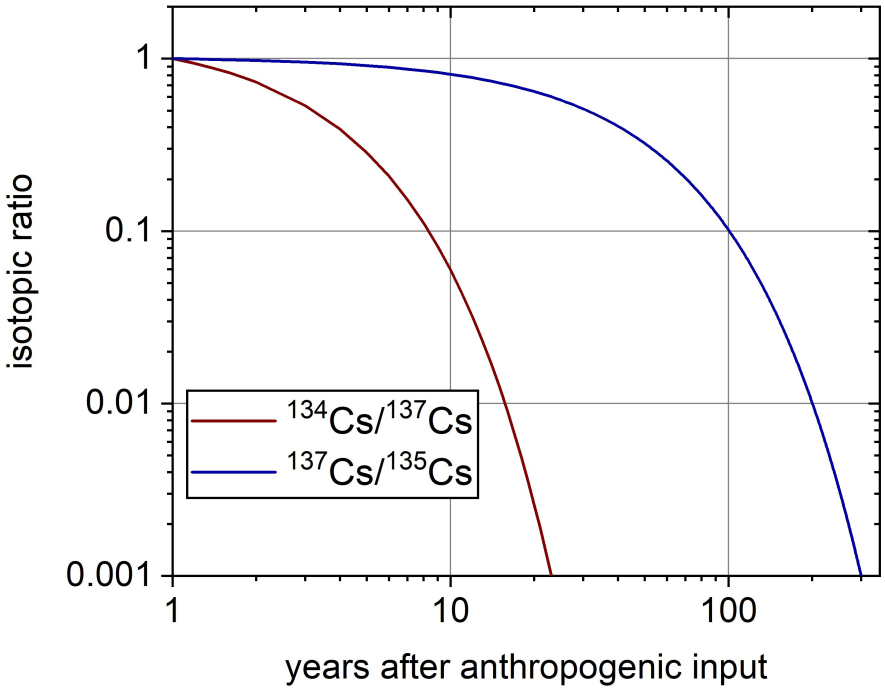

Figure 1.1: Comparison of long-time effects on the two mostly for nuclear forensic investigated isotopic ratios of radiocesium. In each case the abundance of the shorter lived isotope is given relative to the longer-lived one.

where ϕ_{th} is the thermal neutron flux and $\sigma(\mathrm{n},\gamma)$ is the thermal neutron capture cross section. As the thermal neutron flux in different nuclear reactors can differ by orders of magnitude, this rate varies massively from facility to facility [5]. For ^{137}Cs there is no such "shielding effect" as for the mass-135 decay chain, thus the ratio of $^{135}\mathrm{Cs}/^{137}\mathrm{Cs}$ can be used as an "isotopic fingerprint".

The $^{135}\mathrm{Cs}/^{137}\mathrm{Cs}$ atomic ratio is useful as a geochemical tracer, indicating nuclear power plant operations [9], dating nuclear fuel burn-up samples [10], performing source term attribution of unknown industrial emission sources [11], studying erosion [12], dating sediments [12], and improving models of anthropogenic radionuclide dispersion in the ocean [13]. Therefore, a database of $^{135}\mathrm{Cs}/^{137}\mathrm{Cs}$ values in the environmental samples would be useful for future applications [4].

^{135}Cs is a pure beta emitter and because of its low end point energy of only 269 keV and the relatively long half-life, it is hardly detectable via radiometric methods. First approaches by TIMS and ICP-MS/MS were done but these methods require extensive chemical treatment and often suffer from effects such as peak-tailing from ^{133}Cs and molecular isobars [14]. While these mass spectrometric methods do not often reach the required limits of detection in means of activity/sample, they achieve very stable measuring environments and great reproducibility.

In fig. 1.2 a modified chart of nuclides is shown to give an overview of the theoretical "shielding effects" for the cesium isotopes but also for better understanding the problems of isobaric interferences when using mass spectrometry for the detection of Cs isotopes.

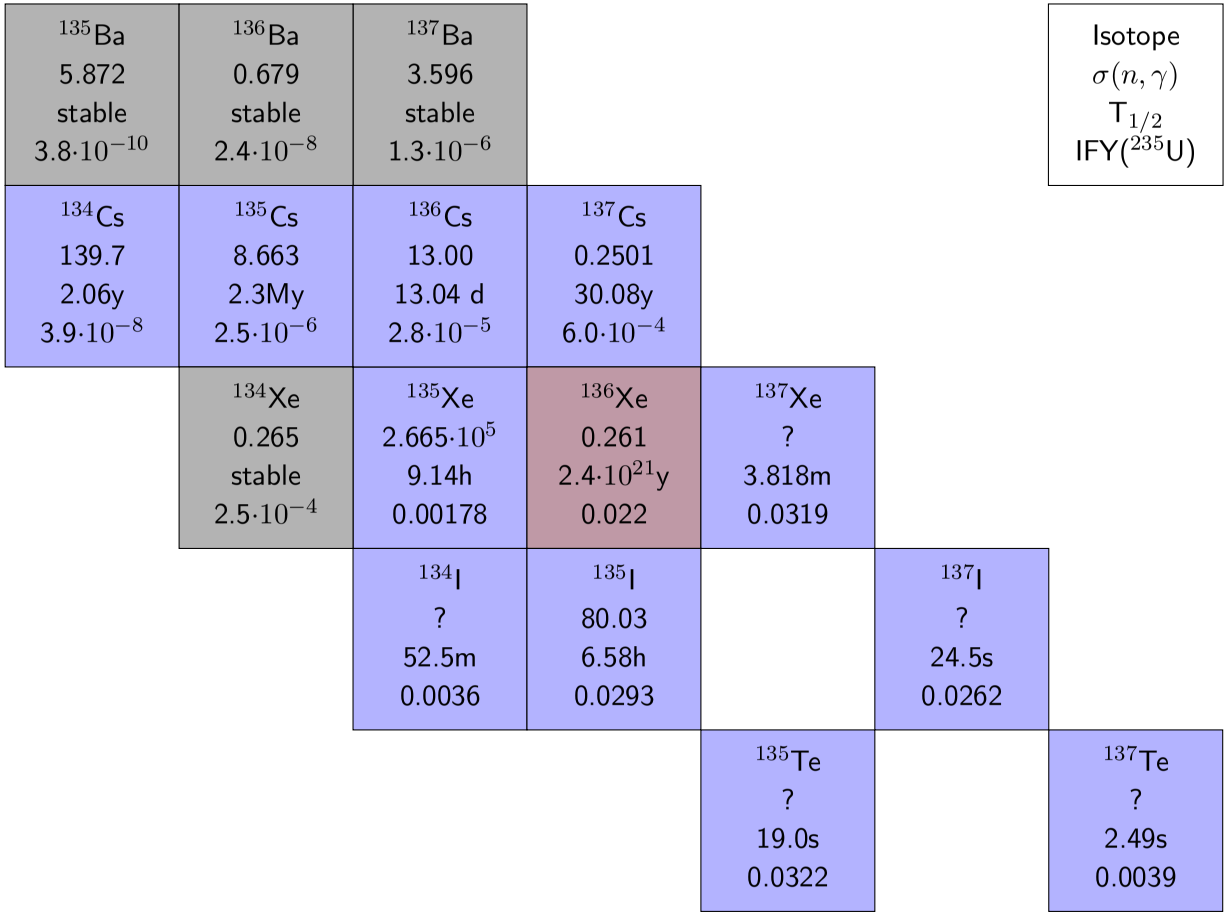

Figure 1.2: This figure shows a picture of the chart of nuclides with information for our interest. In the first line of each square we see the name and the mass number of each isotope. The second line reads the thermal neutron capture cross section $\sigma(n,\gamma)$ in barn. For isotopes marked with a "?" in this line, $\sigma(n,\gamma)$ is not known. The third line displays the half-life. The fourth line gives the independent thermal neutron fission yield of ^{235}U for each isotope. The colour code shows the decay mode, were grey means stable, purple means long-lived so that it can be seen as nearly stable and blue means β^- decay. [7]

2 Introduction

2.1 Production of ^{135}Cs and ^{137}Cs

^{135}Cs and ^{137}Cs are produced anthropogenically in nuclear fission reactors but also naturally by spontaneous fission from ^{238}U. For the anthropogenic case, the so called "reactor poison" ^{135}Xe alters the isotopic ratio ^{135}Cs/^{137}Cs, which makes it possible to identify certain reactors and differentiate it from the natural occuring background.

2.1.1 Fissile and fertile nuclides

Only few nuclides have a sufficiently high cross section to undergo neutron induced fission. These nuclides are distinguished in two groups: fissile and fertile nuclides [15]. Fissile nuclides will undergo fission when a neutron of any energy hits the nucleus. Fertile nuclides however only have a small probability to undergo fission but rather catch a neutron and transform directly or over radioactive decay into some fissile nuclide. The probability for fertile nuclides to undergo fission is strongly dependent of the neutron energy which induces the fission process. For neutrons in the MeV range, fertile nuclides also undergo fission [15].

Fig. 2.1 displays the difference between fertile and fissile nuclides by means of their cross section for thermal neutron energy (25 meV). ^{238}U and ^{240}Pu both can catch a neutron and in the case of uranium transform over two consecutive beta decays into ^{239}Pu, a fissile nuclide, and in the case of ^{240}Pu directly into ^{241}Pu which is also a fissile nuclide.

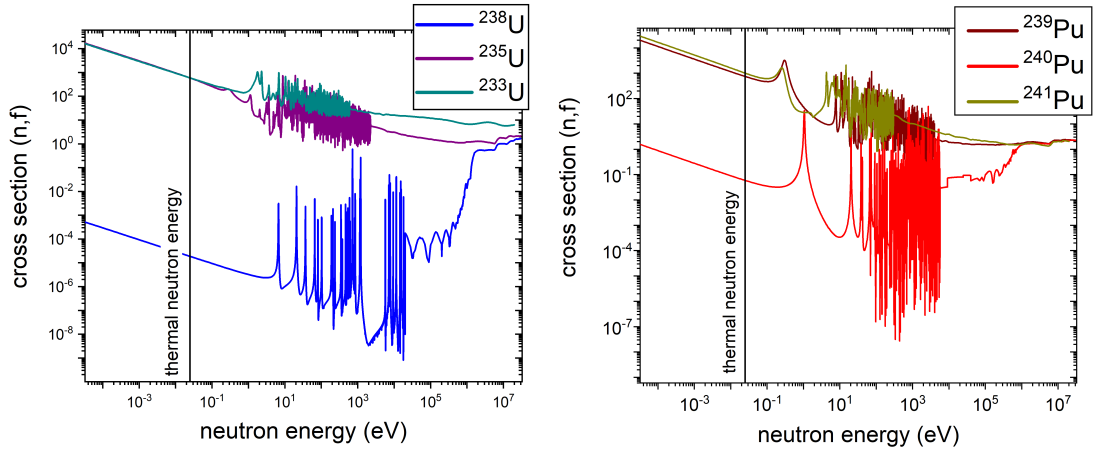

(a) (b)

Figure 2.1: (n,f) cross sections for a) uranium and b) plutonium. For both elements one can distinguish between fertile and fissile materials. Data taken from JANIS, JENDL 4.0 [16]

An important nuclide for a long-term sustainability of nuclear power is the fertile nuclide ^{232}Th. After catching a neutron, it decays to ^{233}U, a fissile nuclide [15]. This is important because of the significantly higher abundance of thorium in the earth's crust ($N_{Th,Crust} \approx N_{U,Crust} \cdot 5.2$ [17]), which assures a longer availability as nuclear fuel.

2.1.2 Fission fragments

In a fission process two new nuclides and on average 2.43 fast neutrons arise for thermal neutron fission on ^{235}U [15]. 99.35% of these neutrons are prompt, so they emerge directly at the fission process within 10^{-14} s. 0.65% are delayed neutrons, which are an accompanying effect of the beta-decay the fission products undergo [15]. There is a small probability of three or even four nuclides emerging from fission, called ternary fission, but in this chapter the focus is on the much more abundant case of only two charged nuclei as fission products. For stability reasons, these two nuclides usually differ largely in mass. The fission yield curve for induced thermal neutrons therefore has two maxima. One at approximately mass 95 amu and the other at about 140 amu. The fission products are neutron-rich and decay towards the valley of stability. The cumulative fission yield gives the integrated probability of

the individual fission yields of one isobar decay chain to occur. The nuclides far from the valley of stability often have half-lives ranging from several orders of magnitude below one second to a few hours. When studying environmental samples, the independent fission yields have been summed up to the accumulated fission yield for every mass chain as the fission yield for the first stable or long-lived nuclide in the decay chain.

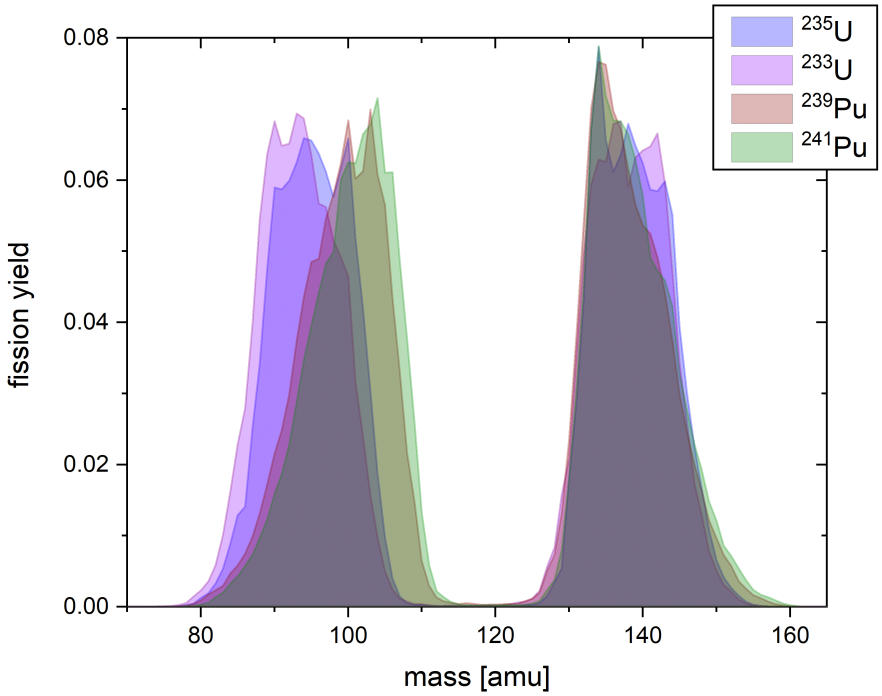

Figure 2.2: Mass vs. yield curve for the four mentioned fissile nuclides. Data taken from JENDL [18] [19]

For radiation protection purposes, especially the medium-lived fission products such as ^{137}Cs and ^{90}Sr, both with approximately 30 yrs of half-life, are of big interest. For AMS the long-lived fission products, which are not detectable over radiometric methods are even more interesting.

In tab. 2.1 an overview of medium-lived and long-lived fission products is given.

Radionuclide	$T_{1/2}$ (yrs)	Fissile Nuclide	AFY [$\cdot 10^{-2}$]	
^{137}Cs	30.0	^{241}Pu	6.649 ± 0.047	medium-lived
^{90}Sr	28.9	^{235}U	5.77 ± 0.59	
^{121m}Sn	43.9	^{239}Pu	0.0031 ± 0.0018	
^{151}Sm	88.8	^{241}Pu	0.913 ± 0.013	
^{113m}Cd	13.1	^{241}Pu	0.00243 ± 0.00065	
^{135}Cs	$1.3 - 3.0 \cdot 10^6$	^{239}Pu	7.617 ± 0.054	long-lived
^{99}Tc	$2.11 \cdot 10^5$	^{239}Pu	6.233 ± 0.090	
^{93}Zr	$1.53 \cdot 10^6$	^{235}U	6.340 ± 0.045	
^{107}Pd	$6.50 \cdot 10^6$	^{241}Pu	4.88 ± 0.39	
^{129}I	$1.57 \cdot 10^7$	^{239}Pu	1.321 ± 0.074	

Table 2.1: Prominent fission products which are important for radiation protection (medium-lived) and AMS detection (long-lived). For the AFY the maximum value for thermal neutron fission on ^{233,235}U and ^{239,241}Pu is displayed. Data taken from [7] [20]

2.1.3 Anthropogenic and natural fission yields

The fission product ratio ^{135}Cs/^{137}Cs varies massively with the number of thermal neutrons emitted in a reactor due to the presence of ^{135}Xe as a precursor in the decay chain of ^{135}Cs. This strong alteration of the isotopic ratio with the thermal neutron flux is unique as ^{135}Xe has the highest thermal neutron capture cross section of all isotopes. The dependence of ^{135}Cs/^{137}Cs on the thermal neutron flux is given in fig. 2.3. While the neutron capture cross section for ^{135}Xe is well studied, there is no known value for the neutron capture cross section of any isobaric precursor of ^{137}Cs. For calculating the ^{135}Cs/^{137}Cs ratio, it was assumed, that $\sigma_{\mathrm{pre}^{137}\mathrm{Cs}}(\mathrm{n},\gamma) = 0$, so only the accumulated fission yield is decisive for the ^{137}Cs abundance. The production yield PY of ^{135}Cs depends only on the thermal neutron flux and is given by

$$\mathrm{PY} = \frac{\lambda(^{135}\mathrm{Xe})}{\lambda(^{135}\mathrm{Xe}) + \sigma(^{135}\mathrm{Xe})\phi_{\mathrm{th}}} \cdot AFY(^{135}\mathrm{Xe}) + FY(^{135}\mathrm{Cs}) \tag{2.1}$$

where $\lambda(^{135}\mathrm{Xe}) = \ln(2)/9.14\,\mathrm{h}$, $\sigma(^{135}\mathrm{Xe}) = \sigma(n,\gamma) = 2.665 \cdot 10^5$ barn, AFY($^{135}\mathrm{Xe}$) = 0.065 is the accumulated fission yield of ^{135}Xe and FY($^{135}\mathrm{Cs}$) $= 2.5 \cdot 10^{-6}$ is the independent fission yield of ^{135}Cs [7].

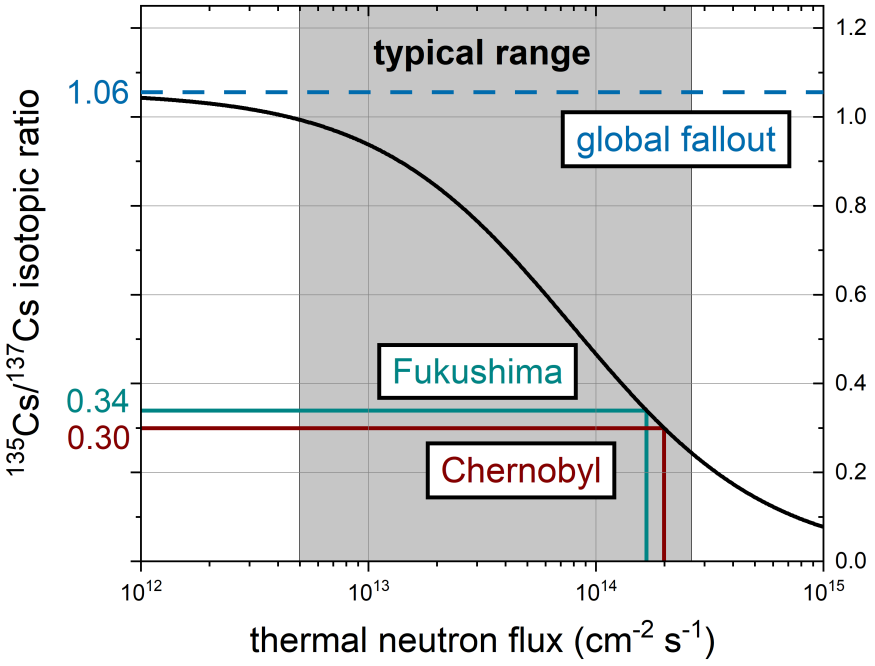

Figure 2.3: Dependence of ^{135}Cs/^{137}Cs as a function of typical thermal neutron fluxes in nuclear reactors [4][14][21]. For this calculation the global fallout value was obtained for $\phi_{\mathrm{th}} = 0$.

The accumulated fission yields for both ^{135}Cs and ^{137}Cs are nearly the same. So, the ^{135}Cs/^{137}Cs ratio from global fallout is well distinguishable from that of reactors and reprocessing plants (see tab. 2.2 and fig. 2.3).

Fissile Nuclide	^{137}Cs AFY [%]	^{135}Cs AFY [%]	Ratio ^{135}Cs/^{137}Cs
^{235}U	6.175 ± 0.034	6.524 ± 0.028	1.0565 ± 0.0074
^{239}Pu	6.605 ± 0.033	7.617 ± 0.054	1.153 ± 0.010
^{241}Pu	6.649 ± 0.047	7.163 ± 0.073	1.077 ± 0.014

Table 2.2: Accumulated fission yields (AFY) for ^{135}Cs and ^{137}Cs for thermal neutrons E = 25.3 meV [2][22]

Natural spontaneous ^{238}U fission with an accumulated fission yield of 0.0521 for ^{135}Cs delivers the natural background of ^{135}Cs [23]. ^{238}U has two decay channels: alpha decay

(α) and spontaneous fission (SF). The half-lives of two competing decay channels add reciprocally:

$$\frac{1}{\tau_{tot}} = \frac{1}{\tau_\alpha} + \frac{1}{\tau_{\mathrm{SF}}} \tag{2.2}$$

The probability of a radioactive decay to happen can be derived from the radioactive decay law as

$$p = 1 - e^{-\lambda t} \tag{2.3}$$

By rearranging this equation and making use of the relation ln(1–p) ≈ – p for small p, we get

$$p \approx \lambda t \tag{2.4}$$

This means that the probability ratio of two decay channels is independent of the time frame, in which it is observed, as long as it is small against the half lives of the respective decays. For ^{238}U this ratio was found to be

$$\frac{p_{\mathrm{SF}}}{p_\alpha} = \frac{\tau_\alpha}{\tau_{\mathrm{SF}}} = 5.4 \cdot 10^{-7} \tag{2.5}$$

Since we know $\tau_{tot} = 4.468\ \mathrm{Gyrs}$ [24], we can calculate the half live for spontaneous fission by plugging this value into eq. 2.2 to be

$$\tau_{\mathrm{SF}} = \left(\frac{p_\alpha}{p_{\mathrm{SF}}} + 1\right) \tau_{tot} = 8.27 \cdot 10^{15}\ \mathrm{yrs} \tag{2.6}$$

The half-live of ^{135}Cs is much shorter than this, which leads to a secular equilibrium:

$$\frac{dN_{^{135}\mathrm{Cs}}}{dt} = \lambda_{\mathrm{SF}} N_{^{238}\mathrm{U}} - \lambda_{^{135}\mathrm{Cs}} N_{^{135}\mathrm{Cs}} = 0 \tag{2.7}$$

which can be rewritten as $N_{^{135}\mathrm{Cs}}/N_{^{238}\mathrm{U}} = \tau_{^{135}\mathrm{Cs}}/\tau_{\mathrm{SF}}$. By considering that only 5.21% of nuclides of the higher mass peak are ^{135}Cs [23], ^{135}Cs/^{238}U can estimated to be $1.5 \cdot 10^{-11}$. As both elements are nearly equally abundant in the earths crust ($\mathrm{N_{Cs}} = 3.7\,\mu g/g$, $\mathrm{N_U} = 2.5\,\mu g/g$ [17]), ^{238}U has a natural abundance of 99.3% and Cs is a mononuclidic element, a natural abundance of ^{135}Cs/^{133}Cs $\approx 6 \cdot 10^{-12}$ can be estimated.

2.2 Accelerator Mass Spectrometry

Accelerator Mass Spectrometry (AMS) is a powerful tool to measure long-lived radionuclides, which are not or only difficult to measure via their radioactive decay. It is capable of determining the mass number of an atom as well as the proton number. The use of an accelerator system as a mass spectrometer improves the abundance sensitivity by many orders of magnitude with respect to standard mass spectrometer without an accelerator.

2.2.1 Ion source

The first of the three fundamental elements of an AMS system is the ion source where negative ions are extracted from the sample material. This process will be explained in more detail in section 3.1.1. The negative ions get accelerated by a voltage of 10 – 100 keV (summing up from the cathode voltage, the extraction voltage ($\mathrm{U_{ext}} = 2-3 \cdot \mathrm{U_{cat}}$) and the source high voltage) before entering the low-energy mass spectrometer. A big advantage of extracting negative ions is, that some isobars of important radionuclides do not form anions, like ^{14}N, an isobar of ^{14}C, ^{26}Mg, an isobar of the cosmogenic radionuclide ^{26}Al, and ^{129}Xe which would interfere with ^{129}I [25].

2.2.2 Principles of mass spectrometry

A standard mass spectrometer consists in principle of two components: a bending magnet (BM) and an electrostatic analyzer (ESA). Ions moving in an electric or magnetic field undergo an acceleration. For a stable circular path to occur, the centripetal force and lorentzian force acting on the particle have to be of equal magnitude.

ESA:

$$\frac{mv^2}{r} = qE \tag{2.8}$$

where m is the mass, q the charge and v the velocity of the ion, r is the radius of the circular path and E the electric field. By rearranging this equation and substituting $T = mv^2/2$, we get

$$\frac{T}{q} = const. \tag{2.9}$$

for a constant electric field and a fixed geometry (e.g. a constant radius). Practically, this means that an ESA selects ions by their energy over charge ratio.

BM:

$$\frac{mv^2}{r} = qvB \tag{2.10}$$

For the bending magnet we can rearrange this equation in the same way and use again $T = mv^2/2$ to obtain

$$\frac{m}{q}\frac{T}{q} = const. \tag{2.11}$$

This equation displays that the ESA and the BM in combination in fact select ions by their m/q-ratio.

2.2.3 Tandem accelerator

After the low-energy mass filter the ions get accelerated in a with SF_6 as insulating gas filled tandem-accelerator to 1 – 15 MeV (depends on the facility and the isotope). In the center of the tandem accelerator electrons get stripped from the negatively charged ions by gas (either helium, argon or oxygen) or foils and the ions therefore get positively charged. The charge state distribution of the outcoming particles is a function of the accelerator voltage and the stripper agent. The positively charged ions now get accelerated in the second half of the tandem by the same potential again. The energy of the ions on the high-energy side is given by

$$T_{\mathrm{HE}} = q_{\mathrm{LE}} \cdot (U_{\mathrm{acc}} + U_{\mathrm{pre}}) \cdot \frac{m_{\mathrm{HE}}}{m_{\mathrm{LE}}} + U_{\mathrm{acc}} \cdot q_{\mathrm{HE}} \tag{2.12}$$

The mass of the cation on the high-energy side of the tandem accelerator can differ from the mass on the low-energy side if the injected ion is a molecule. Molecules in high positive charge states are not stable because of their lack of binding electrons. Generally, small molecules of light elements are not stable in the charge state 3^+, since the coulomb explosion is considered to be energetically more favorable over molecular ionization [26][27][28]. There are few molecules, which were observed to form molecules in the 3^+ charge state such as CS_2^{3+} or COS^{3+} but they do not interfere with common applications in AMS. However, for heavier elements Lachner et al. 2013 [28] at the TANDY AMS facility at ETH Zürich showed that 3^+ charged molecules as UH^{3+} and

ThH^{3+} can deliver some relevant background, especially for low-energy AMS actinides measurements. In general, the stripping process in AMS has the huge advantage that it totally suppresses molecular interferences by choosing a suitable charge state. Molecular isobars are a major problem in other mass spectrometric techniques. On the high-energy side again a mass spectrometer filters the ions by m/q before they enter the detector.

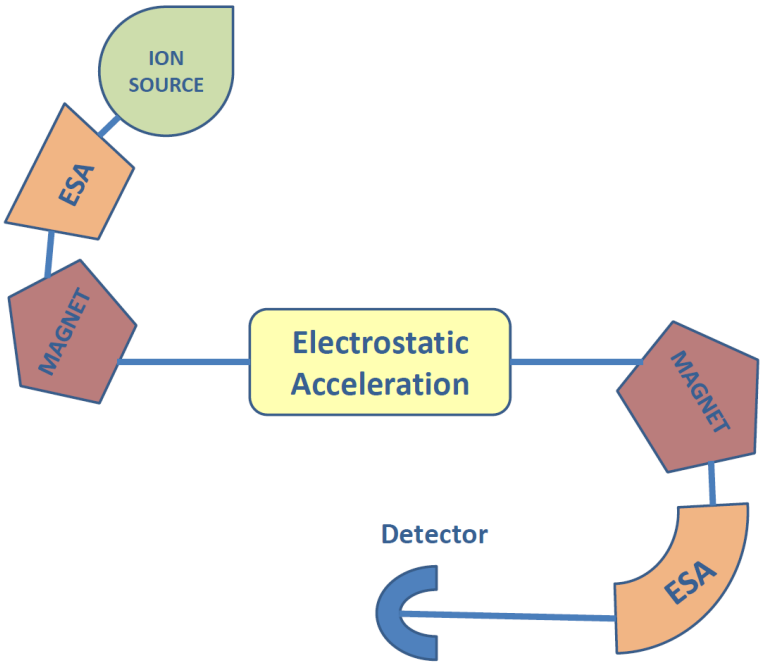

Figure 2.4: Schematic view of an AMS facility

Elemental isobars are the major problem to overcome in most AMS measurements. So called m/q-interferences (e.g. $^{135}Cs^{3+}$ and $^{90}Zr^{2+}$, both have m/q = 45) can be avoided by a suitable charge state selection or distinguished in the detector system if the m/q-interference is not too intense.

2.2.4 Detection system

A standard method in AMS is to distinguish between isobars by their different energy loss in matter since the stopping power is dependent on the nucleus charge number. The heaviest radionuclide which can be measured this way is ^{99}Tc, where the intense stable ruthenium is blocked by a gas-filled magnet [29]. Through charge exchange interactions between the ions and the gas each element forms a different average charge

state and can thus be separated by the magnet [30]. For ^{10}Be measurements ^{10}B gets stopped in a gas cell or a foil before even entering the detector [29].

2.3 Vienna Environmental Research Accelerator

The **V**ienna **E**nvironmental **R**esearch **A**ccelerator (**VERA**) was installed 1995 and is operated by the Isotope Physics group of the University of Vienna. The initial scientific goal was to establish an AMS facility which is capable of serving the dual purpose of interdisciplinary research but also technical development and education for students. The heart of the facility is the 3 MV pelletron accelerator by NEC. A pelletron is a type of electrostatic accelerator which resembles the van de Graaff generator. The electric charge is generated by a mechanical transportation system made of a chain of pellets, which are short conductive tubes connected by links of insulating material [31].

The first isotopes which were measured at VERA were ^{14}C, ^{26}Al and ^{10}Be for radiocarbon dating, nuclear cross section research and paleoclimatology [32]. Today, thanks to additions such as the high-energy ESA, the ILIAMS setup, a switching magnet and another high-energy magnet to the "original" VERA, a vast variety of isotopes can be measured. An overview is given in tab. 2.3 .

now possible at VERA	^{10}Be	^{129}I	^{14}C	^{233,236}U	^{26}Al	$^{239-244}$Pu	^{36}Cl
candidates for ILIAMS	^{53}Mn	^{93}Zr	^{99}Tc	^{107}Pd	^{135}Cs	^{90}Sr	^{182}Hf

Table 2.3: Overview of already routinely measured isotopes at VERA, where ^{26}Al und ^{36}Cl are measured with ILIAMS. The second line displays further candidates in different progression stages for ILIAMS which should be eventually added to the routinely measured repertoire of VERA.

Presently VERA has two MC-SNICS (Multi-Cathode Source of Negative Ions by Cesium Sputtering). One of these ion sources is located on the ILIAMS beamline and used for the CsF_2^- measurements. The low energy side of the VERA structure consists further of two electrostatic analyzers (ESA) and two magnets where one is equipped with a magnet chamber to obtain fast switching between beams of similar mass. After the magnet chamber three offset Faraday cups are located for detection of similar masses as

the injected ion mass. These can also be used by choosing a suitable magnet chamber voltage to monitor the transmission through the accelerator by fast switching between the two beams. On the ILIAMS-beamline the ion cooler and Faraday cups before and after it are installed to monitor the transmission through the cooler (see dotted box in fig. 2.5) [33]. On the high energy side two 90°-bending magnets and one switching magnet are placed. After the first high energy magnet offset cups are disposed as on the low energy side. Before the switching magnet an isobutane-filled ionization chamber is installed for detecting ^{14}C, ^{26}Al, ^{135}Cs, ^{36}Cl and ^{90}Sr. After the switching magnet there are four different beamlines: at -20° for proton induced x-ray emission (PIXE), at 0° for ^{10}Be detection, at +20° an additional bending magnet which is followed by a Bragg-type detector and at +40° a multi anode ionization chamber for ^{36}Cl detection. An overview of the whole facility is given in fig. 2.5.

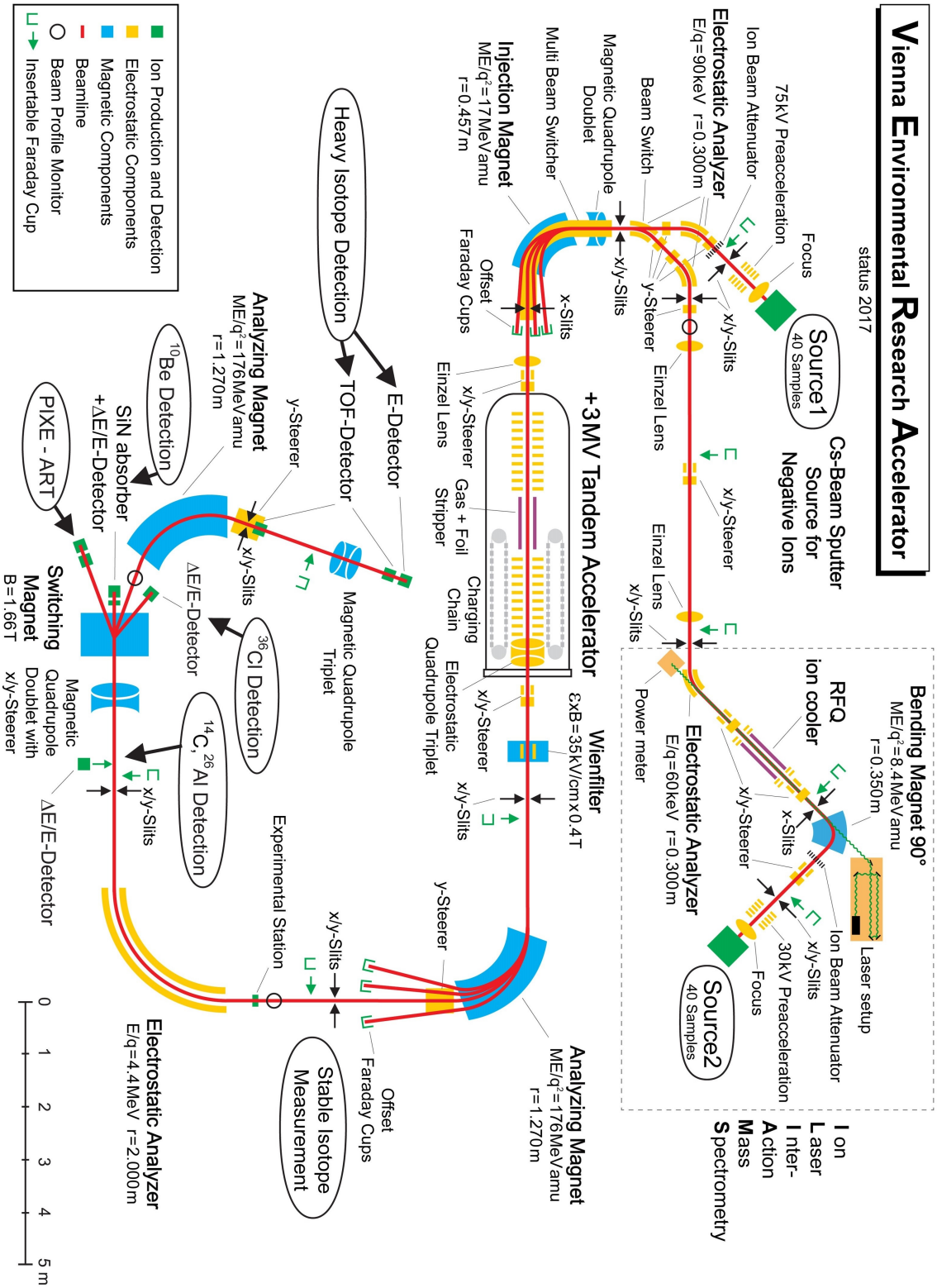

Figure 2.5: Scheme of the whole VERA facility

2.4 ILIAMS

ILIAMS stands for **I**on **L**aser **I**nter**A**ction **M**ass **S**pectrometry, and is an additional isobar selecting element after the second ion source at VERA [33]. ILIAMS itself was installed in 2015 after testing it on an independent test bench not connected to the accelerator [6] [34]. ILIAMS overcomes isobaric problems via laser photodetachment. The negative ions get extracted from the ion source, momentum over charge separated by an analyzing magnet and afterwards injected into the ion cooler. The ion cooler is the key element for isobar suppression. It is basically a linear Paul trap containing four radiofrequency rods and four guide electrodes (see fig. 2.6) [6].

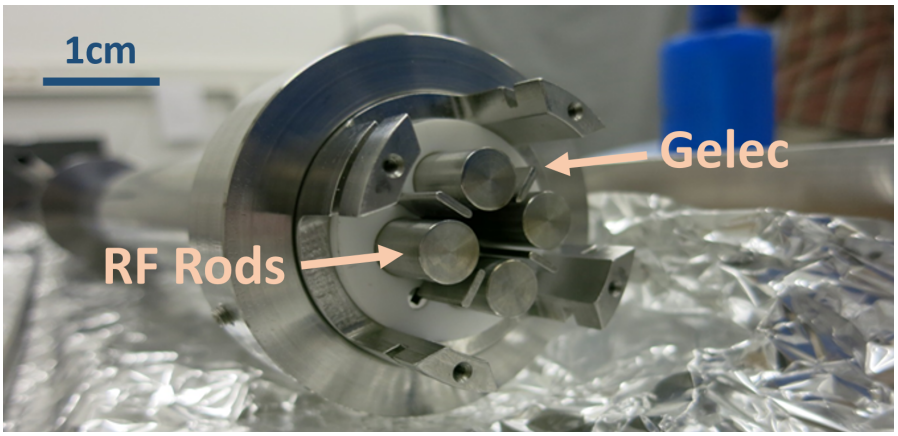

Figure 2.6: Internal structure of the ion cooler with the the four radiofrequency rods (RF Rods) and the four guide electrodes (Gelec)

2.4.1 Linear Paul trap and Mathieu equations

In a linear Paul trap the force acting on a charged particle is defined by the electric field, which is induced by an electric potential.

$$\vec{F} = q\vec{E} = -q\nabla\Phi \tag{2.13}$$

At VERA the ions see no potential in the beam direction (which is represented by the z-coordinate), so only the two-dimensional Paul trap will be discussed here. As

a boundary condition Φ has to fulfill the Laplace equation $\Delta\Phi$=0. This leads to a potential of the form

$$\Phi(t) = \frac{\Phi_0(t)}{r_0^2}(x^2 - y^2) \tag{2.14}$$

where (x, y) is the plane orthogonal to the beam direction and $\Phi_0(t) = U_0 + V_0\ cos(\omega t)$.

r_0 is half the diameter between two opposing RF-Rods. When choosing circular rods instead of hyperbolic ones, only an approximation of a quadrupole field can be achieved. The best approximation is done for $r/r_0 = 1.1468$ and since the rods have a radius of $r = 5.00$ mm, this yields a value of $r_0 = 4.37$ mm [35].

The key element is Φ_0 as oscillating electric potential with a static component. Since this induced field is inhomogeneous, the net force, which acts on the particle is not necessarily zero. Dependent on the amplitude and on the frequency of the oscillating field, this can lead to confinement or to divergent behaviour. Ions that move along the z-axis get pushed towards the optical axis in x-direction but diverge in y-direction. By reversing the polarity of the electrodes a net effect of focusing can be achieved by choosing a suitable frequency ω [36].

The mechanical analogue is a sphere, which lays near the top (which means in our case that $\sqrt{x_0^2 + y_0^2} \neq 0$) of a saddle-formed surface in a gravitational potential. If the surface were kept static, the sphere would just roll down, but by rotating the saddle with the right frequency the sphere can be upheld (fig. 2.7).

The equations of motion for one charged particle in vacuum can be written as the so-called "Mathieu equations" [38]

$$\frac{d^2u_j}{dt^2} + (a_j - 2q_j\ cos(2\tau))u_j = 0 \tag{2.15}$$

where $u_j = (x, y)$ for $j = 1,2$ and a and q are the so-called Mathieu parameters. The Mathieu parameters are antisymmetric for x and y, since the potential is antisymmetric in the x-y-plane.

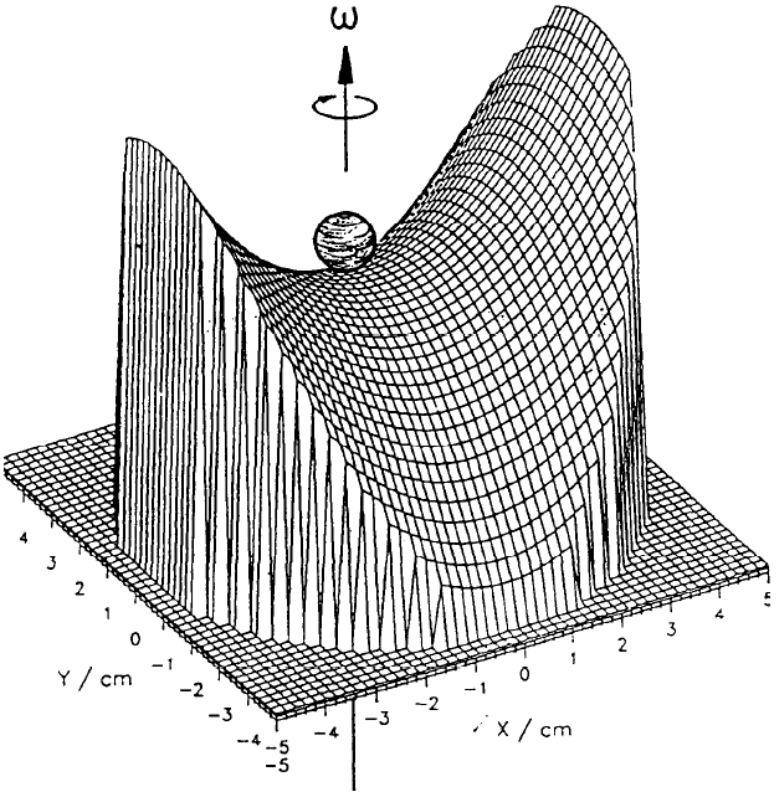

Figure 2.7: Mechanical analogue for the linear Paul trap [37]

$$a_x = -a_y = \frac{8QU_0}{mr_0^2\Omega^2} \tag{2.16}$$

$$q_x = -q_y = -\frac{4QV_0}{mr_0^2\Omega^2} \tag{2.17}$$

By solving the Mathieu differential equation, one gets bounded solutions, which physically means ion confinement for $\tau \to \infty$ dependent on the values a_j and q_j. A section of the boundary conditions in the $a-q$-plane is shown in fig. 2.8. For practical reasons the stable area near the origin is most important because the ions are supposed to be cooled to the center of the potential [36].

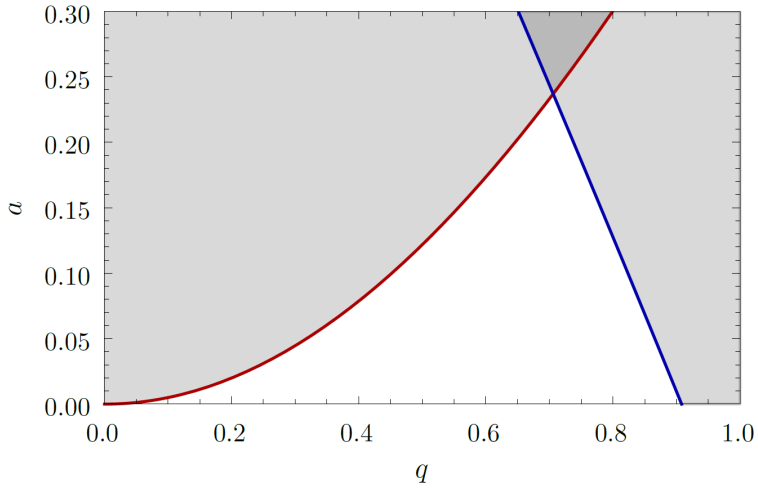

Figure 2.8: Stable solutions (a,q) of the Mathieu equation in x- and y-direction are depicted in white. Stable solutions in only one of the two directions are given in light-gray. Solutions in the dark-gray area are unstable. Figure taken from [35].

In case of ILIAMS no static component of Φ_0 is applied, so it acts only as a ion guide and as a weak mass filter. This means, that $a = 0$ and we can only move on the q-axis in the region $0 < q < 0.908$. Martschini et al. [34] showed that a stable ion current is achieved at $q = 0.5$, whereas for all q below 0.3 and above 0.7 no confinement is reached (see fig. 2.9).

The equation for the Mathieu parameter is

$$m = \frac{4\ QV_0}{q\ r_0^2\Omega^2} \propto q^{-1} \tag{2.18}$$

With this we can calculate, that e.g. for ^{35}Cl the mass interval, for which confinement is achieved, is 25 – 58 amu.

$$35\,\text{amu} = \frac{4\ QV_0}{0.5\ r_0^2\Omega^2} \rightarrow \frac{4\ QV_0}{r_0^2\Omega^2} = 17.5\,\text{amu} = const. \tag{2.19}$$

$$m_{\text{max}} = 17.5\,\text{amu}/0.3 \approx 58\,\text{amu} \tag{2.20}$$

$$m_{\text{min}} = 17.5\,\text{amu}/0.7 = 25\,\text{amu} \tag{2.21}$$

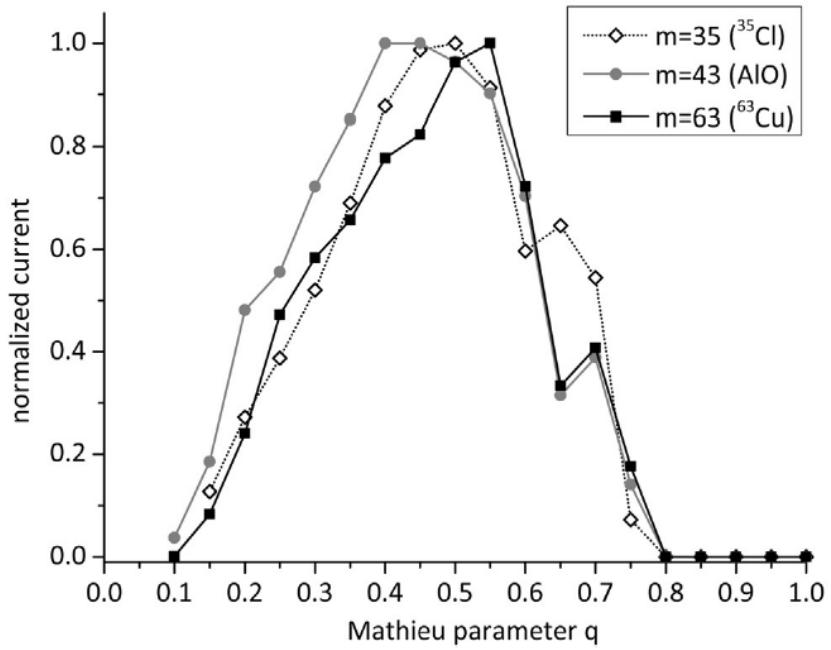

Figure 2.9: Transmission through the ion cooler for three ions with the RF voltage kept constant and varying RF frequency. The ion cooler acts as a weak mass filter in the interval of $0.3 < q < 0.7$ (FWHM) [34].

Ions of higher or lower mass cannot pass the ion cooler in the ^{35}Cl settings.

The ion cooler is equipped with a power supply, which can decelerate the incoming ions electrostatically by a voltage of up to 30 kV. For focussing on both sides of the ion cooler lenses are placed, which, especially on the entrance of the cooler, have to compensate for angular divergence due to deceleration. A weak electric field guides the ions to the exit of the cooler where the ions get reaccelerated to –30·Q keV. Inside the cooler buffer gas is dampening the ion motion but also suppressing isobars due to collisional detachment and chemical reactions with the gas. The chemical and the kinetical effect can be reinforced by mixing the helium with O_2 – gas or H_2 – gas.

2.4.2 Buffer gas cooling

Ions in the ion guide are moving in two overlapping periodic paths. The micro-motion, which is caused by the RF-field and the macro-motion which is simply the oscillation

of the particle, often called secular motion. The energy of the micro-motion is fixed, since the radio-frequency is fixed, so the only way to reduce this energy is to damp the amplitude of the macro-motion or the secular motion, respectively. So, by collisions with a light gas on average a cooling effect is visible [36].

Buffer gas cooling is a wide spread technique but mostly done with positive ions, since the ionization potential is often one order of magnitude higher than the detachment energy. For negative ions to survive the entrance into the cooler, the center of mass energy must not exceed the electron affinity of the incoming ions. This has to be taken into account for choosing the power of the electrostatic deceleration and the injecting ion energy [34].

$$E_{ion} \cdot \frac{m_{gas}}{m_{gas} + m_{ion}} < EA \tag{2.22}$$

2.4.3 Laser photodetachment

The process of photodetachment is described by the equation

$$A^- + \gamma \rightarrow A + e^- \tag{2.23}$$

where A is some atom or molecule and γ is a photon with adequate energy to detach the electron. This detachment is a threshold process, so it is sufficient that $E_\gamma >$ EA, where EA is the so called electron affinity. The probability for this process to happen depends on the cross section σ, the photon flux ϕ and the interaction time t [34]. The number of depleted ions is given by

$$N_{depleted} = N_0 \cdot (1 - e^{\sigma \phi t}) \tag{2.24}$$

The cross section around the threshold energy is modelled by the Wigner law, where c is some proportionality constant and L is the angular momentum of the photoelectron.

$$\sigma(E) = \begin{cases} 0, & E < EA \\ c \cdot (E - EA)^{L+1/2}, & E > EA \end{cases}$$

A sketch for L = 0 is given in fig. 2.10. One can see by experiment that a green laser with 532 nm, respectively 2.33 eV has a suitable energy for detachment of the unwanted isobar in the case of CsF_2^-. The cross section for detachment for the extracted Cs-molecule is virtually zero, while there is a non-zero cross section for detachment for the Ba-molecule. Experimental electron affinities for both molecules are not known at the moment.

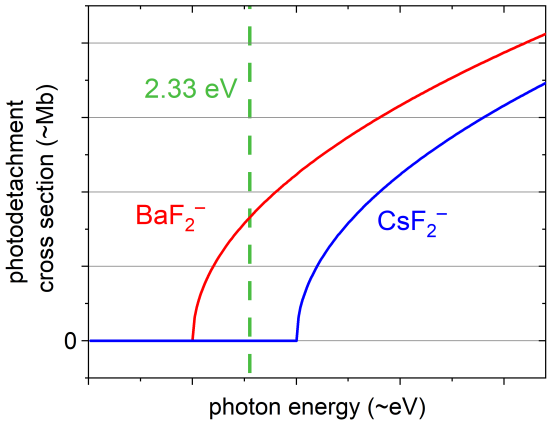

Figure 2.10: Photodetachment cross sections for a $s = 0$ wave $\rightarrow \Delta L = 0$

Armin Shayeghi from the Philip Walther group [39] has performed an estimation for the vertical detachment energy VDE. In general, the VDE can be used as an upper limit for the electron affinity (see fig. 2.11). While the electron affinity is defined as the energy difference between the two ground states of the anion and the outcoming neutral atom/molecule, the VDE is defined as the energy difference in the ground state of the anion and an excited state of the neutral atom/molecule (see fig. 2.11)

The VDE's are $VDE_{CsF_2^-} = 3.88$ eV and $VDE_{BaF_2^-} = 0.61$ eV, which matches with our observations from experiment. The green laser at 2.33 eV photon energy detaches the barium-difluoride and does not affect the cesium-difluoride. With these estimations, we can calculate the collisional detachment energy for CsF_2^- to ≈ 170 eV. This means that the ions have to get decelerated just below this energy for entering the cooler and still achieve maximum suppression for BaF_2^-.

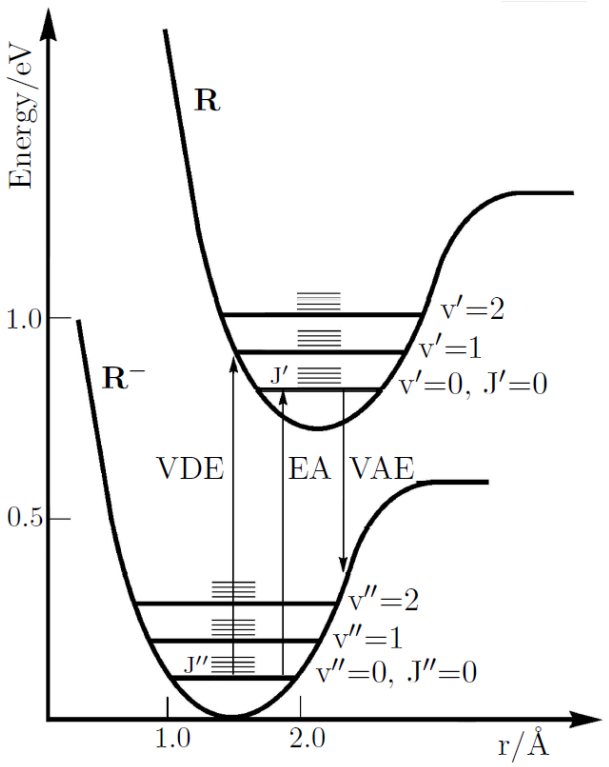

Figure 2.11: Qualitative diagram of the surface potential of a molecule. VDE and VAE as upper and lower limits for estimating the electron affinity EA are indicated by the arrows [40].

3 ^{135}Cs - State of the Art

In this chapter an overview of the status of ^{135}Cs-measurements, respectively ^{135}Cs/^{137}Cs measurements, around the world will be given with a special focus on the status of the measurements at VERA prior to this master thesis.

3.1 Previous Cs measurements at VERA

The preliminary work was done 2014-2015 by Magdalena Kasberger in her diploma thesis [41]. At that time, the ILIAMS-Setup was not yet installed at the second injection beamline at VERA. The aim of the work was to establish a suitable ion current output, to maximize the transmission through the accelerator and to find a way to distinguish between cesium and barium in the detector. A big issue at the beginning was the handling of the ion source. In all other AMS measurements at VERA, a cesium oven is used for sputtering. To avoid a distortion of the isotopic ratio by diluting the sample material with the stable cesium from the oven and maybe introducing a new source for radiocesium, a different sputter agent had to be found and tested [41].

3.1.1 Rubidium sputtering

Cesium and rubidium are both alkali metals and process therefore as electron donator. The efficiency of negative ionization is one key parameter of every AMS measurement, which leads to the fact that the processes in the ion source are well studied (see e.g. [42]). A schematic image of the functionality of an ion source is given in fig. 3.1.

The sputter agent, e.g. cesium or rubidium, in the heated oven vaporizes and rises trough a heated capillary to the volume in front of the sample. The Cs/Rb atoms get ionized on a hot tantalum surface, the so-called ionizer, and get accelerated towards

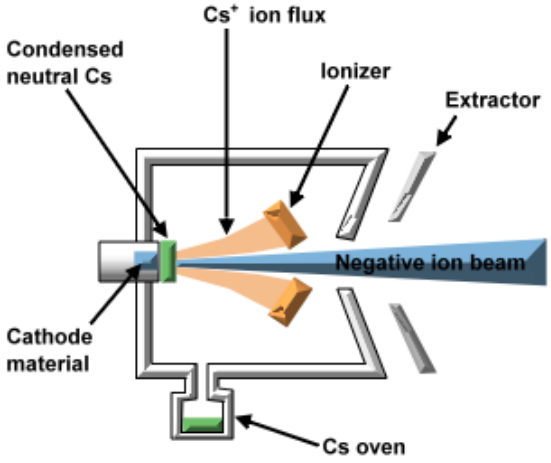

Figure 3.1: Schematic picture of the functionality of an AMS ion source. Picture taken from [43]

the sample by the cathode voltage. There, these ions "knock out" atoms from the sample material and as these atoms move through a neutral condensed Cs/Rb-layer and the Cs/Rb plasma, which have built in front of the sample, the sample atoms get negatively charged due to the electron donator behavior of Cs/Rb. The acceleration of the sample anions is done by the same voltage as for the positively charged sputter agent but now in the opposite direction.

Tests for already established AMS molecules/atoms were made to characterize the sputtering efficiency for the rubidium sputter agent [3]. For many anions it makes no difference at all and the biggest differences occur for carbon and beryllium with a reduction of the output by a factor of ≈ 2.

Element	ex. Anion	Rb [μA]	Cs [μA]
C	$^{12}C^-$	17	30
Be	$^{9}Be^{16}O^-$	0.8	1.5
F	$^{19}F^-$	0.65	0.65
Al	$^{27}Al^-$	0.1	0.1
Cl	$^{35}Cl^-$	6	6
Cs	$^{133}Cs^-$	0.01	-

Table 3.1: Ion current output of different established AMS-elements [3] [41]

3.1.2 Matrix material tests

The matrix material is some additional mixed in metallic material to maximize ion current output and ionisation efficiency of the measured isotope. It can also increase the thermal and electric conductivity and help therefore minimizing cross contamination in the ion source.

Barium has a very low electron affinity of 0.14 eV, so it hardly forms negative ions [44]. So the first approach was to extract Cs^-. As a chemical carrier cesium sulfate (Cs_2SO_4) was chosen due to its high melting point. Cs^- was more intense than the also forming oxides CsO_X^-. Additionally barium does form oxides much better, so no suppression in the ion source was achieved.

Eliades et al. [45] at the IsoTrace Laboratory report a reduction factor of $BaF_2^-/CsF_2^- = 5 \cdot 10^{-4}$. For this molecule to form tests with mixing Cs_2SO_4 with PbF_2 and LaF_3 were made. While Kasberger could not reproduce the reduction factor of Eliades, she only found $BaF_2^-/CsF_2^- = (8 \pm 3) \cdot 10^{-2}$, CsF_2^- was clearly the molecule to investigate further [41]. CsF_2^- is a superhalogen molecule, which promises stable and high ion currents but also high electron affinities. This makes the production of superhalogen anions easy, as long as the precursor neutral atom is stable enough and a highly fluorinating matrix material is added [46].

3.1.3 Suppression in the detector

Without ILIAMS the differentiation between barium and cesium has to take place in the detector. Barium has stable isotopes on mass 130, 132, 134, 135, 136, 137 and 138, cesium on the other hand only on mass 133. For comparison the bary centers of ^{132}Ba and ^{134}Ba in the Multi-Anode Ionization Chamber (MAIC) were linearly interpolated to simulate ^{133}Ba and compare it with ^{133}Cs. The measurements were done at an ion energy of 25.8 MeV in 8^+ state. There is far too little difference in the barycenters to distinguish the two elements, even at that high energy (see fig. 3.2).

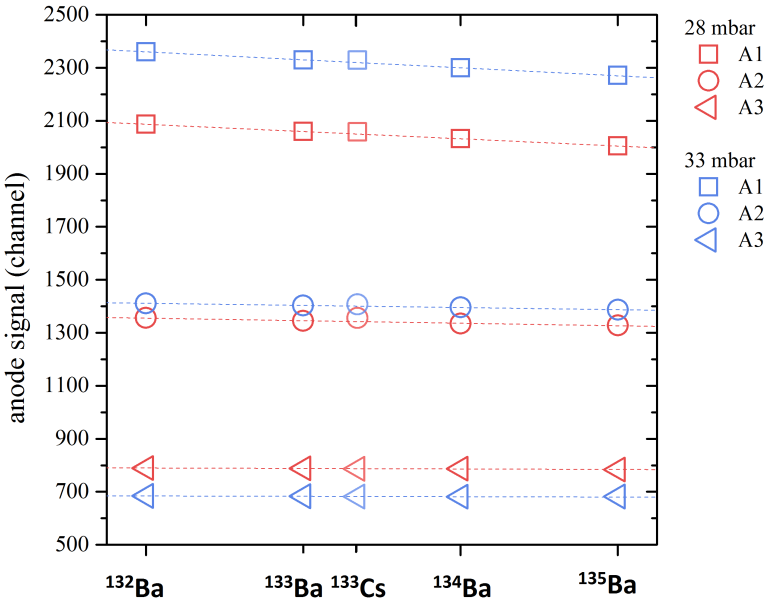

Figure 3.2: Comparison between the barycenters in the MAIC detector. ^{133}Ba was simulated by linear interpolation of ^{132}Ba and ^{134}Ba. Figure taken from [41]

3.1.4 Chemical suppression in the ion cooler

In the time between the end of the masters thesis of Magdalena Kasberger and the beginning of this one, tests for chemical suppression in the ion cooler were made. The normally used helium buffer gas was mixed with oxygen in the ratio He:$O_2 = 100$:1. Since barium forms oxides very well, BaF_2^- could catch an additional oxygen atom and gets therefore separated at the bending magnet after the ion cooler due to its now different mass to charge ratio [47].

Similar behavior was already seen for $^{182}HfF_5^-$, where a suppression of the isobar $^{182}WF_5^-$ of a factor $W_{He}/W_{He+O_2} \approx 160$ with respect to pure helium buffer gas was achieved while the hafnium stayed nearly unaffected by the additional oxygen input of He:$O_2 = 30$:1 [48].

Unfortunately we do not see the same effect for barium. Scans over the buffer gas pressure show that pure helium has a slightly higher damping effect per millibar than the helium-oxygen mixture (see fig. 3.3). Further tests with hydrogen admixture are planned. In this master thesis all measurements were performed with pure helium.

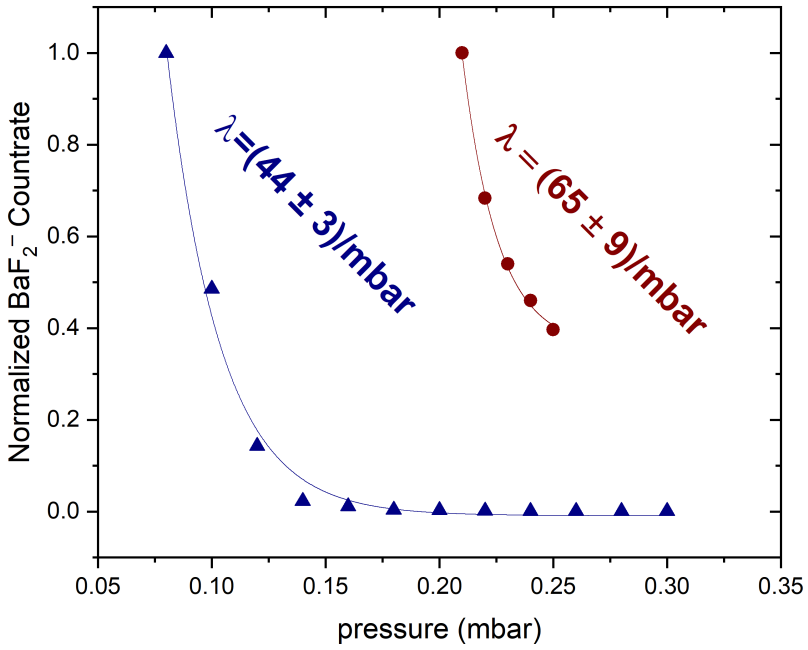

Figure 3.3: The ion current decreases exponentially in dependence of the buffer gas pressure. Since this means the damping λ is constant one can fit an exponential curve and determine its value. The damping is larger for pure helium (in red on the right) than for He+O_2 (in blue on the left). Here the intensity of a $^{135}BaF_2^-$-beam is shown normalized to its maximal value in the measurement series. Data taken from [49]

3.2 AMS measurements of ^{135}Cs at the IsoTrace Laboratory

At the IsoTrace AMS Laboratory in Toronto operated by the University of Ottawa first measurements of Cs by AMS were done. The original goal was to apply this technique

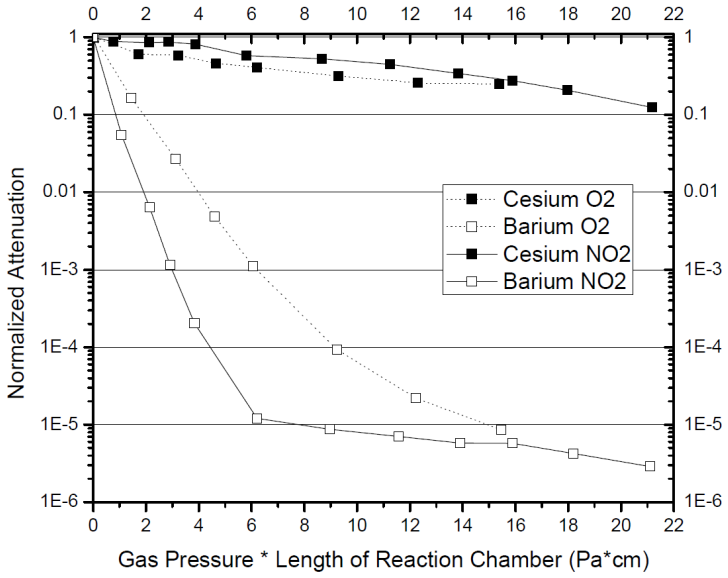

Figure 3.4: MacDonald et al. [50] at the IsoTrace Laboratory found barium suppression factors of $2 \cdot 10^{-5}$ by using O_2 and NO_2 in their reaction cell. Due to the different configurations of the ISA gas cell (15 cm long for NO_2 vs. 23 cm long for O_2) the suppression curve is represented as attenuation per cm of gas cell per Pa of O_2 pressure [50].

to measure the half-life of ^{135}Cs [50]. The isobar problem there is solved with the so called ISA (Isobar Separator for Anions): In this gas-filled reaction cell the negative ions get decelerated and captured in a radiofrequency field. There they react with, in the case of Cs, NO_2 or O_2 [50] [47]. The ions then get reaccelerated into the AMS system. Barium reacts much stronger with oxygen than cesium. By analyzing the outcoming ions again by their m/q ratio the interfering isobar gets separated. Barium suppression of $2 \cdot 10^{-5}$ was achieved that way (see fig. 3.4). In contrast to VERA, cesium sputtering was performed for these measurements. ^{134}Cs was added to the sample and by tracking the amount of this isotope through sample preparation and measurement, the absolute amount of ^{135}Cs could be calculated.

The abundance sensitivity reached by this method is in the order of $^{135}\text{Cs}/^{133}\text{Cs} = 10^{-10}$, which is similar to TIMS (see chapter 3.3.2). The limitation of the method is the high cross contamination in the ion source [50].

3.3 Cs measurements by other mass spectrometric approaches of environmental samples

In this section a short overview on other measurement techniques (ICP MS, TIMS and NAA) and results for determining the $^{135}Cs/^{137}Cs$ ratio is given.

3.3.1 Inductively Coupled Plasma Mass Spectrometry (ICP MS)

ICP MS is a widely used technique to determine trace isotopes in environmental sciences. The samples are introduced into a plasma and ionized positively. The emerging ions are filtered by means of m/q. The problem of peak tailing of stable isotopes to trace isotopes is limited by the use of a quadrupole as a mass filter [14]. A common way to suppress molecular isobars (e.g. $^{95}Mo^{40}Ar^{+}$, $^{119}Sn^{16}O^{+}$ for $^{135}Cs^{+}$ measurements) is to introduce a reaction cell between two quadrupole mass filters, where the chemical reactions should change the m/q of either the interfering isobar or the isotope of interest. This technique is called ICP MS/MS or triple quadrupole ICP MS and is commercially available since 2012. For ^{135}Cs N_2O is chosen as a reaction gas since barium likes to form oxides, whereas the cesium doesn't react [51] (see fig. 3.5).

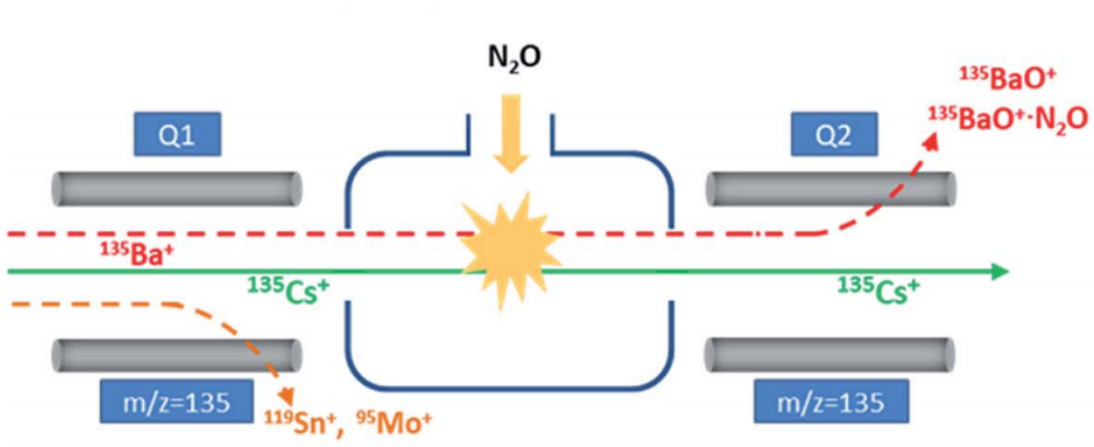

Figure 3.5: Scheme of a ICP MS measurement for ^{135}Cs. Picture taken from [51]

The limit of detection for most ^{135}Cs and ^{137}Cs measurements with this method is $< 1{\cdot}10^{-8}$. This is sufficient to measure environmental samples which were contaminated by global fallout, but requires large amounts of up to 40 g soil [14] [51]. Zhao et al. [46] propose that an abundance sensitivity of ^{135}Cs/Cs $\approx 10^{-14}$ is required for most oceanic and environmental samples.

3.3.2 Thermal Ionization Mass Spectrometry (TIMS)

TIMS is a measurement technique with higher precision than ICP MS. The suppression of barium happens mostly in the ion source by choosing a suitable filament current at which cesium gets ionized and barium does not due to its higher ionization potential. The abundance sensitivity is about ten orders of magnitude in terms of ^{135}Cs/^{133}Cs which is sufficient to neglect the peak tailing effect. Other matrix materials (mostly Ca, Fe, Al, Mg, K, Na & Rb [14]) suppress ionization of cesium. So, chemical separation of these elements is absolutely necessary.

The precision of TIMS measurements at a level of 10 fg of ^{135,137}Cs is still less than 10 %, which makes it practicable for comparing reference materials of environmental samples [14].

3.3.3 Neutron Activation Analysis (NAA)

By irradiating cesium samples with neutrons, one can determine the ^{135}Cs/^{137}Cs isotopic ratio, by measuring the gamma lines of ^{136}Cs at 340.55 keV, 818.51 keV and 1.048 MeV [52]. The number of ^{137}Cs before and after the irradiation will stay nearly constant, since the thermal neutron capture cross section for ^{135}Cs is by a factor $\approx$ 35 larger than that of ^{137}Cs [7]. For normalization and as irradiaton monitor ^{134}Cs and its 604.72 keV and 795.86 keV gamma lines can be used [53]. ^{134}Cs is shielded by ^{134}Xe and has a very low independent fission yield, therefore it can only be produced by neutron capture of ^{133}Cs. The limit of detection for this method is similar to that of ICP MS and basically limited by the uncertainties, which arise from the evaluation of the peak area due to the presence of the Compton background and of other Cs isotopes [54]. ^{134}Cs is the most interfering gamma radiator and is disturbing the low ^{135}Cs countrate [21]. A spectrum of two samples measured by NAA is shown in fig. 3.6.

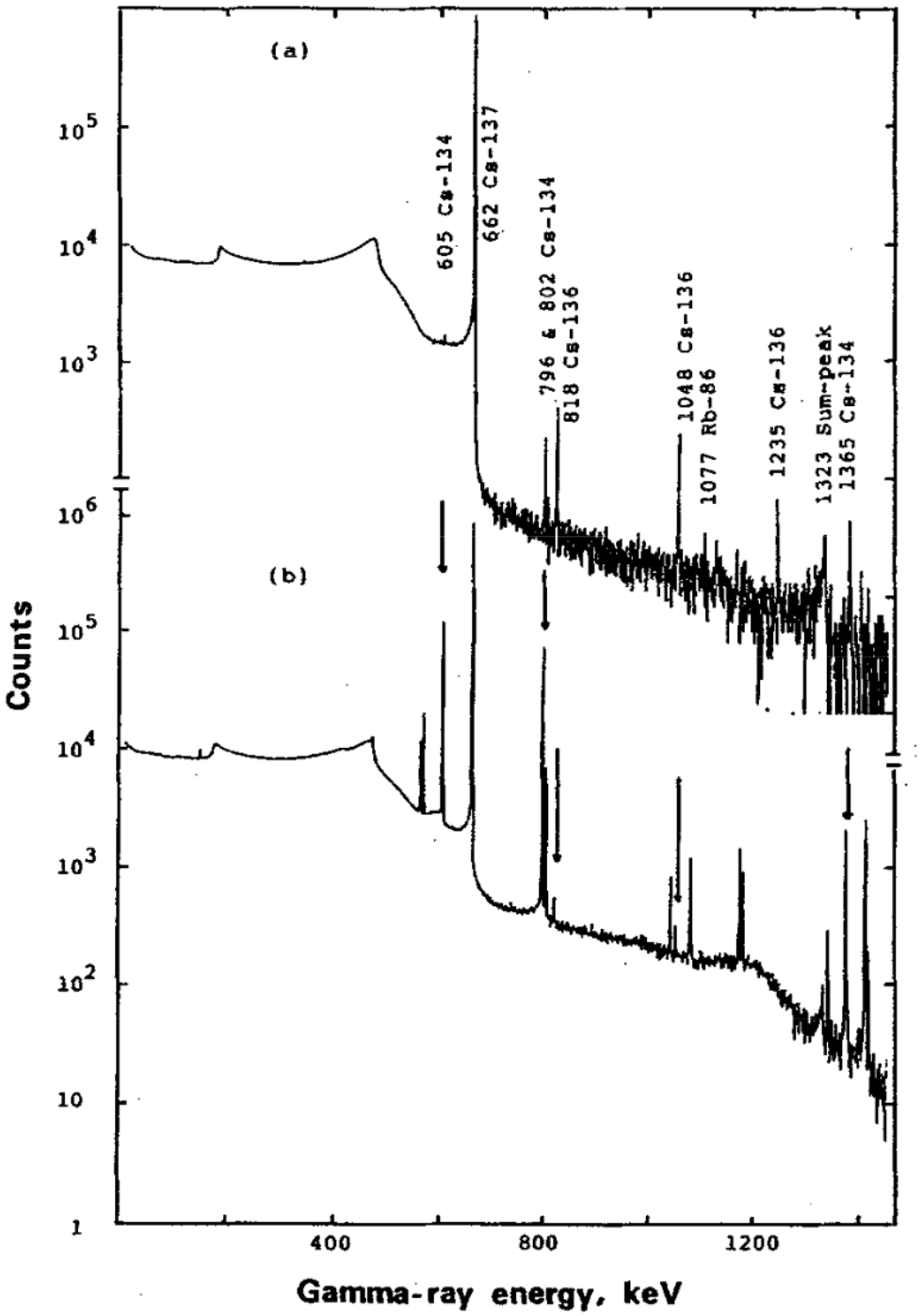

Figure 3.6: Two samples measured by Chao et al. [21] by neutron activation analysis: a) a ^{137}Cs tracer and b) a sample from a nuclear power plant.

Conclusion

TIMS is the most advanced measurement technique at the moment for ^{135}Cs measurements. It delivers great reproducibility at ^{135}Cs/^{133}Cs abundance sensitivities in the order of 10^9 or higher which makes it possible to measure the ^{135}Cs/^{137}Cs ratio in Chernobyl contaminated samples. However, for measuring environmental samples the abundance sensitivity would have to be improved by another four orders of magnitude.

4 AMS measurements for determining ^{135}Cs/^{137}Cs with ILIAMS

In this chapter results of AMS measurements with ILIAMS and isobar suppression via laser photodetachment will be shown. Further, an overview of used materials will be given. The measurement principle and tuning process will be explained, results on isobar suppression, isotopic ratios found in in-house reference materials and finally test-runs on IAEA reference materials will be presented.

4.1 Choice of basic materials

4.1.1 Cesium carrier and barium spike

Carrier are materials which do not contain any radioactive isotopes. The purity of the carrier material therefore is crucial for the blank level of an AMS measurement. The carrier is necessary to obtain macroscopic amounts of a sample. If we would extract the cesium from a sample without adding a Cs carrier no macroscopic amount of material could be found in typical environmental sample sizes. Spikes are materials where the interfering isobars are mixed in on purpose. Spikes are produced for tuning processes but also for measuring and monitoring the isobar suppression via laser photodetachment throughout a measurement.

As a carrier for the reference materials but also for the blank and the barium spike cesium sulfate and cesium chloride were used. These materials are in crystalline form and hygroscopic [55][56]. In first measurements no difference in ion current output of

CsF_2^- (Cs_2SO_4/CsCl+PbF_2) or blank level was seen, so Cs_2SO_4 was further used due to its higher melting point of 1010 °C in contrast to 646 °C of CsCl.

Further, two spikes were mixed in atomic ratios of Ba:Cs = 1:100 and 1:10. Especially the 1:100 mixture spike is of high importance, as it represents the abundance one expects in natural samples quite well without any chemical Ba separation. BaF_2 was used as barium carrier [57].

4.1.2 In-house reference material

Reference materials have predetermined ratios of the radioactive isotope with respect to one stable isotope. Isotopic ratios of unknown samples can be corrected by the measured isotopic ratio of the reference material. The alteration in the isotopic ratio of the sample is mostly due to losses of the rare isotope through the accelerator.

As a reference material in Cs measurements at VERA, a ^{137}Cs solution from the UK Amersham radiochemical centre which was available in the institute's collection from 1964 was used. The ^{137}Cs activity is measured by gamma radiation. For the ^{135}Cs abundance no values are known. Therefore, this reference material can only deliver a nominal $^{137}Cs/^{133}Cs$ value, but no $^{135}Cs/^{133}Cs$. The solution was mixed with 0.1M HNO_3 and milli-Q water to obtain a 100 Bq/ml and a 2 Bq/ml solution.

The radioactive solution was mixed with a solution of a Cs carrier in milli-Q water, so a definite $^{137}Cs/^{133}Cs$ ratio can be obtained. In this master thesis materials were used with $^{137}Cs/^{133}Cs$ ratios ranging from 10^{-8} down to 10^{-11}.

4.1.3 Fluoride extraction

As we want to extract the superhalogen molecule CsF_2^- we need to introduce fluorides into the sample matrix. For this purpose, tests with different Cs_2SO_4:PbF_2 ratios were made. To obtain the right ratio, samples with Cs_2SO_4:PbF_2 mass ratios from 1:2 up to 1:6 were made and their CsF_2^- current was measured. The ion current was measured after the first magnet BMI1-1 (see fig. 2.5) and a wide mass range was chosen for measuring the Cu_2^- and Cu_3^- ion current extracted from the cathode material (see fig.

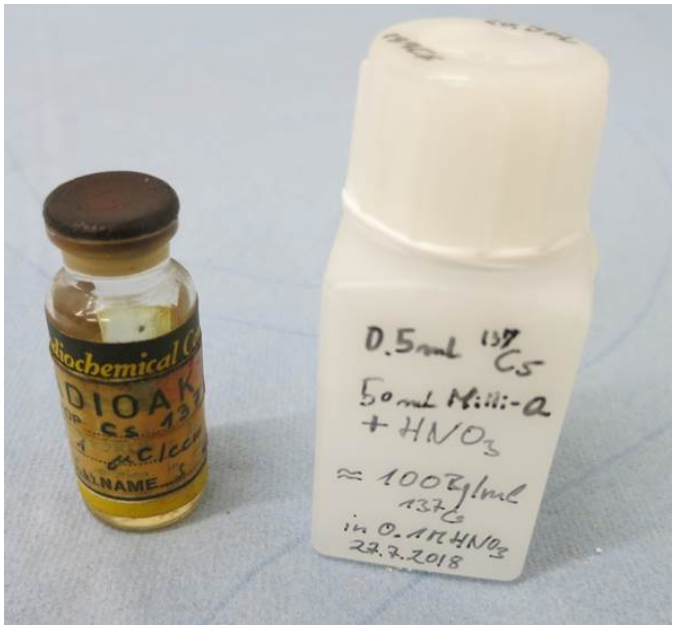

Figure 4.1: Picture of the original Amersham ^{137}Cs solution and the 100 Bq/ml solution mixed with milli-Q water and 0.1M HNO_3 [49]

4.2). These Cu-signatures can help identifying the general output of the ion source and can serve therefore as a normalizing factor. The normalization follows

$$\text{"}\mathrm{CsF_2 : Cu}\text{"} = \frac{\mathrm{CsF_2}}{\mathrm{Cu_2 + Cu_2F + Cu_3}} \tag{4.1}$$

where always the highest peak for each Cu-signature was taken. Since we assume that every target was sputtered optically equal, there should be no difference between a normalization to the integral of each Cu-signature or only the highest peak of each Cu-signature.

The ion currents for this measurement are shown in 4.3. There was no additional copper mixed to the samples. The high Cu currents only arise from the sample holder and the sample wheel, which are both made out of copper. PbF_2 from Sigma-Aldrich was used to obtain CsF_2^- [58].

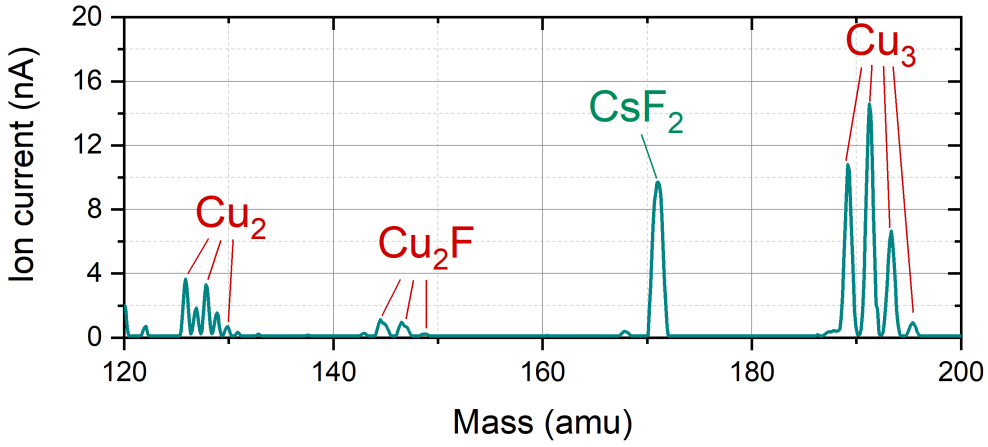

Figure 4.2: Massscan of a PbF_2:Cs_2SO_4 = 2:1 sample. Copper signatures are clearly visible and are used to monitor the general ion source output.

PbF_2:Cs_2SO_4 (mass)	CsF_2^- (nA)	CsF_2:Cu
2:1	9.72	0.53
3:1	16.82	0.79
4:1	15.71	0.76
5:1	17.99	0.74
2:1	7.57	0.42
3:1	17.20	0.84
4:1	10.49	0.67
5:1	11.64	0.58
6:1	17.39	0.79
6:1	17.05	0.75

Table 4.1: Ion current output for the massscans in the beamtime Cs1912a in chronological order for the CsF_2^--peak and the normalization factor. The chronological order is important for interpreting this data, since the introduction of fluorine into the ion source can have a delayed effect on the ion current output. That is also the reason why at first samples with low normalized PbF_2 proportions were measured.

The desired molecule CsF_2^- builds much better in the ion source for PbF_2 mass proportions > 0.75. From there, the additional mixed in fluorine seem to have no big influence on the molecule building mechanism.

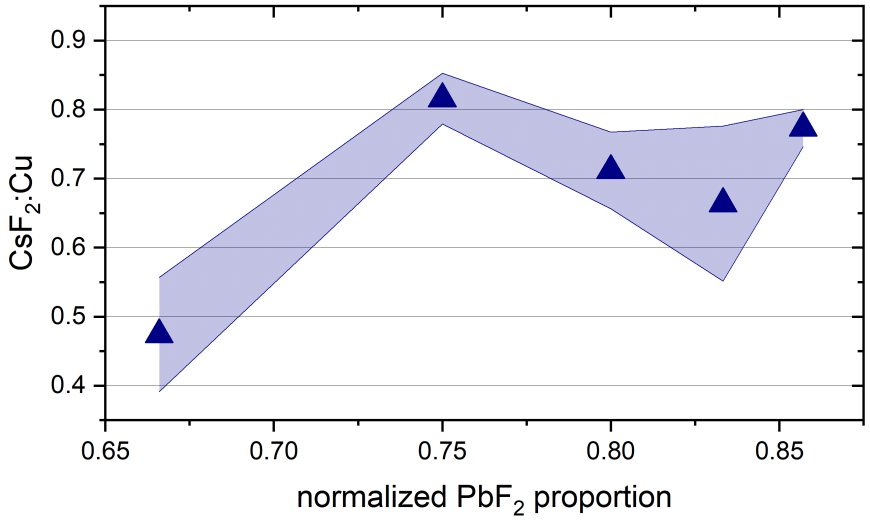

Figure 4.3: Normalized CsF_2^- ion currents in dependence of the additionally mixed mass proportion of PbF_2 (e.g. PbF_2:Cs_2SO_4 = 4:1 leads to a mass proportion of 0.8 and so on). The shaded area depicts the uncertainty of the measurements.

4.2 Transmissions

The transmission through the accelerator is estimated as

$$\text{Transmission} = \frac{^{133}\text{Cs}^{3+}}{3 \cdot \ ^{133}\text{CsF}_2^-} \tag{4.2}$$

A single value for the transmission is of no great value, since it depends strongly on the pressure of the stripper medium and the terminal voltage with which the ions get accelerated. In fig. 4.4 the transmission is plotted against the stripper gas pressure in the measuring cell after the accelerator tank. A maximum can be found at about $5 \cdot 10^{-8}$ mbar with 20 % transmission on average. A theoretical maximum value of about 25 %, where no losses due to kinetic reactions occur, is nearly reached at this pressure.

For the stripper medium and accelerator voltage Lachner et al. 2015 [3] reported tests with helium and argon in the range from ≈ 2.1 MV to ≈ 3.0 MV using Cs^- (see fig.

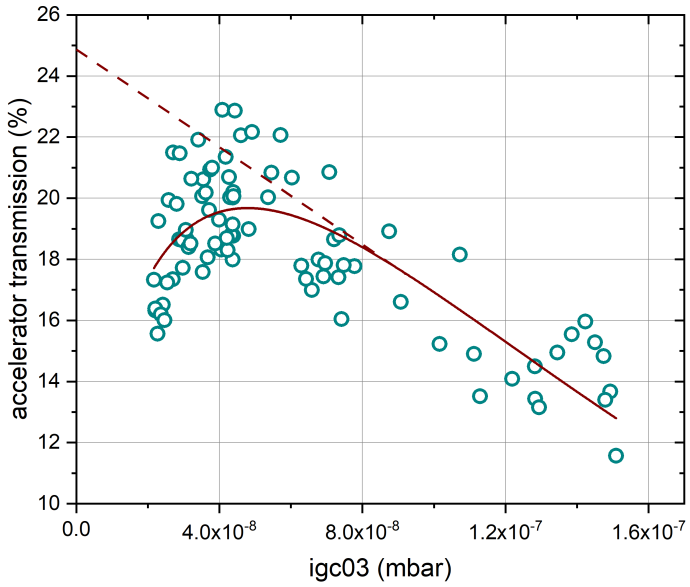

Figure 4.4: The accelerator transmission depends on the stripper gas pressure. For this test helium was used. While low gas pressure does not lead to stripping in the 3^+ state, the curve shows linear regression for higher pressure values, since the losses due to collisional effects increase. The linear part can be extrapolated to obtain a theoretical 3^+ yield, where no losses due to collisions occur. The function used for fitting here is: $T = ax^b\ exp(-cx)$, where the fit parameter a, b and c have no physical meaning.

4.5). The low charge states 2^+ and 3^+ are clearly the options to further investigate. The two stripper agents helium and argon show no major differences. Measurements will be repeated with CsF_2^- injection. Since we do not need high energies to separate isobars in the detector the most efficient settings would be at around 2.1 MV or even lower, 2^+ with Argon stripping.

The transmission through the ion cooler is calculated by dividing the m/q selected ion current after the ion cooler by the injected current. The transmissions through the ion cooler are known to be current dependent [59]. Source regulation has therefore to be performed to have similar ion current outputs before injecting into the cooler to maintain the principles of a reference measurement. The ion current at VERA can be

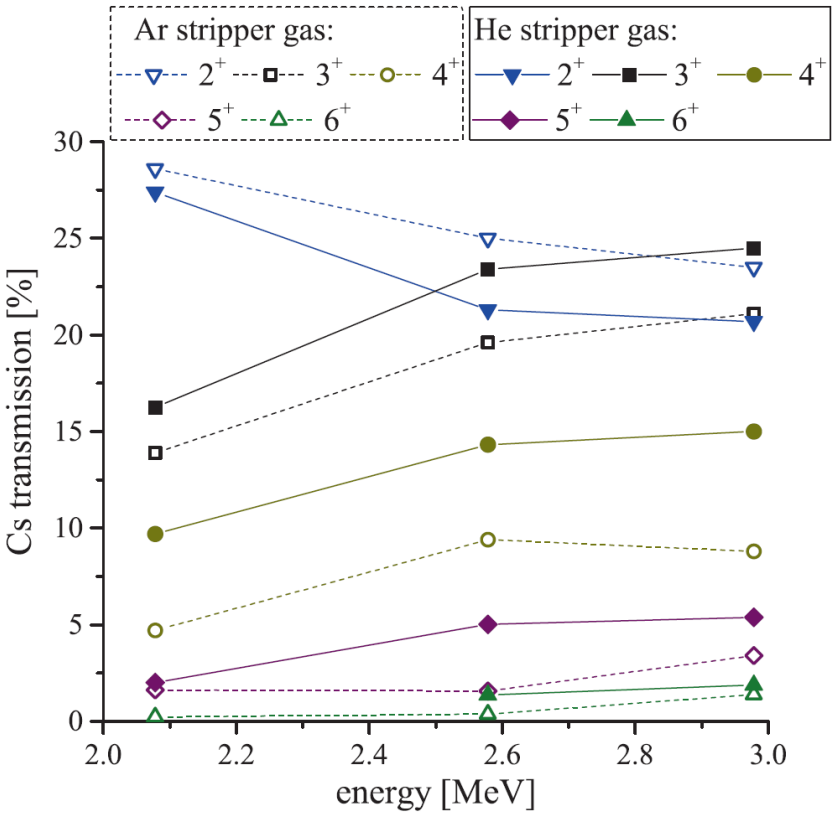

Figure 4.5: Transmission trough the accelerator for helium and argon stripping injecting Cs^-. For lower voltages here no shorting rods were applied, but steerers and lenses were adjusted. Figure taken from [3]

influenced by three parameters: the temperature of the oven, the power of the ionizer and the temperature of the lineheater. The lineheater is a small capillary connecting the Cs/Rb reservoir with the volume in front of the sample wheel. For Cs measurements source regulation would lead to some problems during the PbF_2 measurements, since the current outputs there are much lower and the regulation on the source would heat up the ionizer/oven/lineheater unnecessarily, so we do not use any regulation. We look to find settings to extract currents at around 100-200 nA after the first magnet, as the ion cooler showed the best transmissions in this range. Values of maximum 34 % were achieved at 0.3 mbar helium. Note that the value on the ion cooler pressure read is only the N_2 equivalent pressure and has to be corrected by a factor 1.24 to obtain the real pressure of the helium gas.

4.3 Cross contamination and blank levels

Cross contamination is the unwanted transfer of small amounts of one sample material to a different one. Cross contamination can have different origins: unsanitary handling at preparing the samples in the chemistry laboratory and at the sample press procedure, but also in the ion source due to source memory effects. In both cases, this mixing of materials alters the measured isotopic ratio. Cross contamination is a major issue for Cs isotope measurements with AMS.

The blank level is the isotopic ratio found on material which only consists of the Cs carrier mixed with PbF_2 without the radiocesium solution.

4.3.1 Rubidium sputtering

As we have no other measurement technique available for determining the ^{135}Cs blank level, we cannot rule out the effects of radiocesium content in the oven and the carrier. But of course we can control the blank level for ^{137}Cs by measuring the 662 keV gamma line. For a sample size of 1 mg, the blank level found in the measurements where Rb sputtering was applied, corresponds to an activity of $\approx$ 0.55 Bq, so a clear signal should be seen with the HPGe detector. But neither for the oven nor for the carrier materials any gamma activity was found. This leads to the conclusion, that high blank levels have their origin in the cross contamination from high reference materials used in the same or in previous beamtimes.

In this master thesis two completely different approaches in terms of negative ion extraction were examined. In the first two beamtimes, the approach of rubidium sputtering was continued as described by Kasberger [41]. With Rb sputtering the extracted CsF_2^--current after the first magnet was only in the order of $\approx$ 10-100 nA (see also tab. 4.1). Further, reference materials with high $^{137,135}Cs/^{133}Cs$ ratios were found to distort the samples with lower isotopic ratios.

Fig. 4.6 displays this effect by showing the nominal versus the measured isotopic ratios. Three different reference materials were mixed with the two different Cs carriers. The

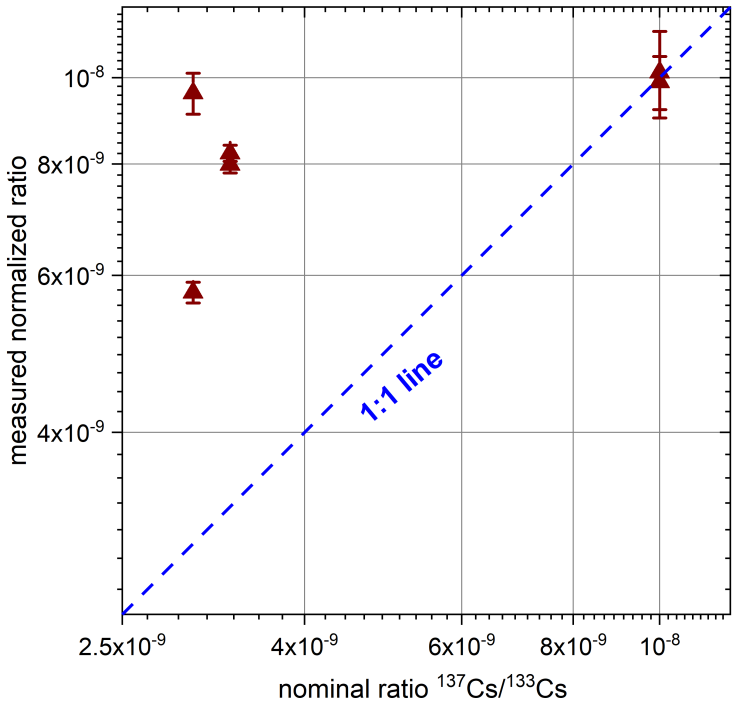

Figure 4.6: Nominal vs. measured ratios normalized to the mean of the highest reference material sputtered with Rb. The low reference materials are far above the 1:1-line. This indicates a mixing effect of the materials in the ion source. Sputtering of source cleaning materials and introducing of lower reference materials into the ion source were done in the following beamtimes to solve this problem.

highest reference material had an isotopic ratio of $^{137}\mathrm{Cs}/^{133}\mathrm{Cs} = 1 \cdot 10^{-8}$ and the lowest $^{137}\mathrm{Cs}/^{133}\mathrm{Cs} = 3 \cdot 10^{-9}$. The relative ratios between those materials were not found to be 10:3 though due to cross contamination. The higher and the lower standards are "mixing" in the ion source, therefore resulting in higher concentrations for the lower reference materials. However, the $^{135}\mathrm{Cs}/^{137}\mathrm{Cs}$ ratio was found to be nearly constant with a mean value of $^{135}\mathrm{Cs}/^{137}\mathrm{Cs} = 1.99 \pm 0.10$ (see fig. 4.7). This is expected, since the samples are all produced from the same radiocesium solution and only diluted differently with the ^{133}Cs carrier, so the cross contamination from one sample to another should have no effect on the $^{135}\mathrm{Cs}/^{137}\mathrm{Cs}$ ratio.

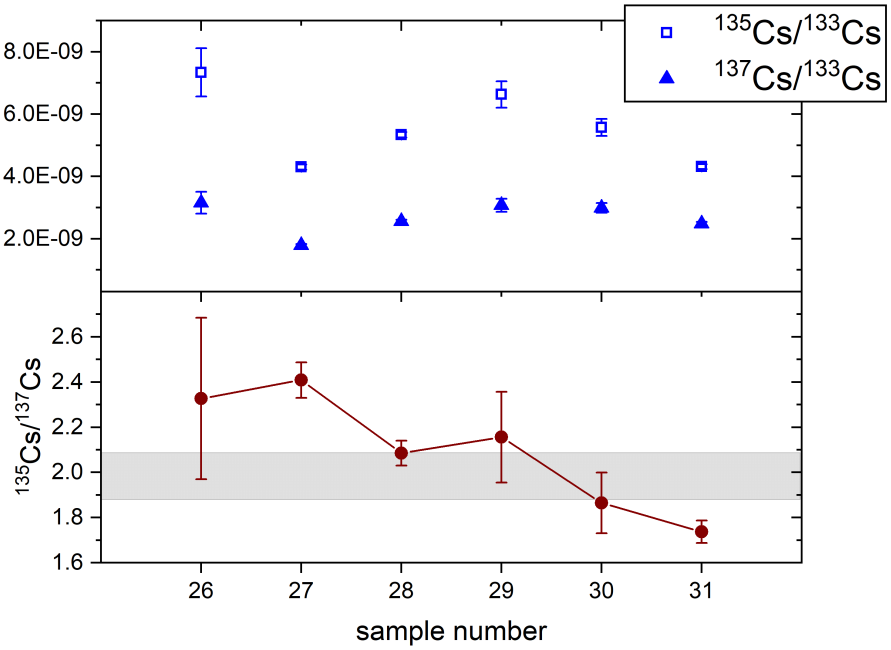

Figure 4.7: Results for the three reference materials measured on the first test runs with ILIAMS. Sample 26 and 29 were Cs_2SO_4 carrier with $^{137}Cs/^{133}Cs = 1 \cdot 10^{-8}$, sample 27 and 30 were Cs_2SO_4 carrier with $^{137}Cs/^{133}Cs = 3 \cdot 10^{-9}$ and sample 28 and 31 were CsCl carrier with $^{137}Cs/^{133}Cs = 3 \cdot 10^{-9}$.

The blank level for these measurements was roughly two orders of magnitude below the nominal isotopic ratio of the highest reference material:

$$^{135}Cs/^{133}Cs = (2.59 \pm 0.18) \cdot 10^{-10} \tag{4.3}$$

$$^{137}Cs/^{133}Cs = (1.69 \pm 0.15) \cdot 10^{-10} \tag{4.4}$$

This corresponds to a $^{135}Cs/^{137}Cs$ ratio of 1.53 $\pm$ 0.18, which is a bit lower than that of the reference material. It is not clear whether the counts on the blank arise from source memory effects, i.e. cross contamination as discussed above, or whether they have different origin. As an external source for radiocesium the cesium oven used in other measurements and the rubidium oven used in this measurement are possible. The Cs carrier could also be a source of radiocesium but this suspicion was refuted by

gamma measurements of the carrier and spike material and no ^{137}Cs gamma activity was found.

4.3.2 Normalization factor

The normalization factor f is the ratio of the nominal isotopic ratio to the measured isotopic ratio of a reference material. It is given by the equation

$$\mathrm{f} = \frac{^{137}\mathrm{Cs}/^{133}\mathrm{Cs}_{\mathrm{nom}}}{^{137}\mathrm{Cs}/^{133}\mathrm{Cs}_{\mathrm{measured}}} \tag{4.5}$$

In most AMS measurements $\mathrm{f} > 1$, due to losses of the rare isotope through the accelerator. It is a powerful tool to monitor the measurement over a period of time and the scattering of the normalization factor can be used as a quality feature of the stability of a measurement. Typical normalization factors for standard AMS isotopes at VERA are given in tab. 4.2. For ^{36}Cl, which is the most successfully measured radioisotope with ILIAMS, the normalization factor is 1.3. [60]

Isotope	^{10}Be	^{14}C	^{41}Ca	^{129}I	^{26}Al	Actinides	^{36}Cl
normalization factor	1.2-1.3	1.2	1.2-1.5	1.3-1.4	1.2	1.2	1.3-1.4

Table 4.2: Typical normalization factors for most relevant AMS nuclides [61] [62]. The value for ^{36}Cl in this table was obtained by classical AMS, although it does not differ significantly from that achieved with ILIAMS.

For the Cs measurements this factor was found to be 1.61 ± 0.20 (fig. 4.8) in measurements without Rb reservoir. For the measurements with Rb sputtering a mean value can not be given due to high cross contamination.

4.3.3 Suppressing Cross Contamination

MacDonald et al. [47] found that this source memory effect is especially severe for Cs (see fig. 4.9).

At VERA, in the beamtime Cs1902a it was found that the ion current output of fluorides from the MC-SNICS ion source is very sensitive to the ionizer power and not so much

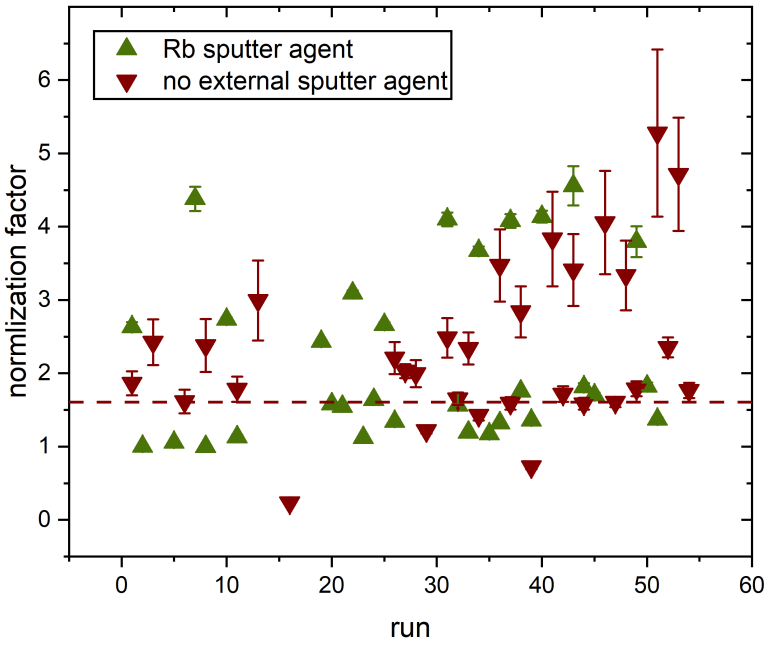

Figure 4.8: Normalization factors for two different measurements: one where Rb sputtering was applied and one without filled and heated Rb reservoir. For the Rb sputtering calculating a mean value would not make sense, because of the systematical error in this dataset, which can be also seen in fig. 4.6. The values at around ≈ 4 derive from the highest reference material, while the lower values are from the lower reference materials. For the dataset without Rb reservoir, all runs were performed on samples with the same nominal isotopic ratio. The mean value for this set is 1.61.

to the oven temperature. Even at low Rb^+-sputter currents, a significant CsF_2^- output was achieved, once enough fluorine was introduced into the ion source by sputtering on pure PbF_2-targets. Similar results had been found by Zhao et al. 2016 [46] for ^{135}Cs in an PbF_2 matrix. They suggested that for fluoride sputtering only low Cs^+ currents are needed since PbF_2 undergoes a so called 'diffuse phase transition' above 250°C and causes high mobility and therefore a high mixing of atoms in the ion source. Similar effects were found for AgF and AgF_2 but no other fluoride. This lead to the idea of a self-sputtering ion source type. Measurements on graphite were made without Cs reservoir and the source was cleaned prior to the measurement to get rid of the

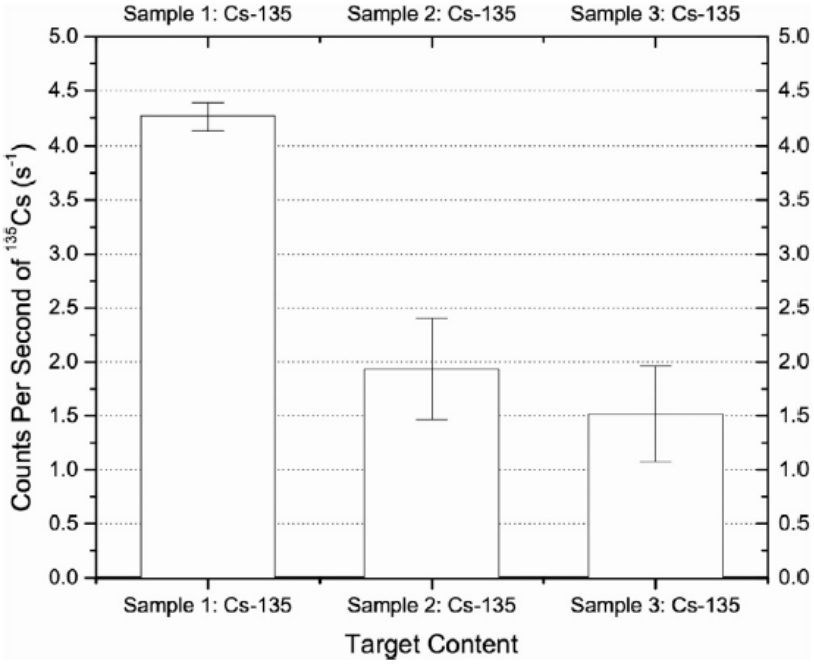

Figure 4.9: Three consecutive measurements at the IsoTrace ISO-AMS system by Macdonald et al. 2015 [47] on three different targets, where, despite the labeling of the three bars, only the first one contains ^{135}Cs. $\approx$ 50% of countrate was transported to the next sample. Similar behaviour was found at VERA, where this factor ranges from 1 % for targets mixed with copper to $>$ 80 % for high reference materials not mixed with copper (see also fig. 4.14)

cesium implanted in the source from other AMS measurements by Zhao et al.: Graphite was measured in a fast-bouncing mode, were the $^{12}C^-$ and the $^{13}C^-/^{12}C^-$ ratio were monitored. After 30 cycles of fast-bouncing a CsF+PbF_2 target was inserted and then again switched back to the graphite target. The goal was to obtain a stable self-sputtering ion beam. The additional sputter ion inserted in the ion source showed that a substantial and sustainable ion beam could be produced for a acceptable amount of time, but also the $^{13}C^-/^{12}C^-$ ratio was altered by the new sputter ion by 5 per mil indicating some major difference in the sputter ions from Cs^+. As always in relative measurements as performed in AMS, it is hoped that a similar measured standard material can correct this offset by normalization (see fig. 4.10) [46].

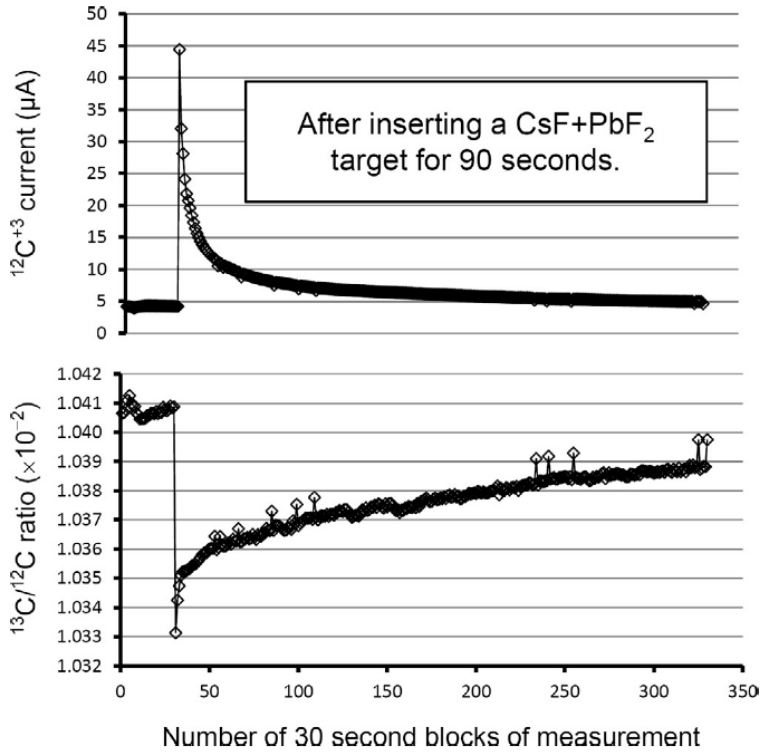

Figure 4.10: Zhao et al. 2016 [46] at the Lalonde AMS Laboratory, Ottawa, showed that a sustainable ion beam can be produced by a self-sputtering process for a period of time. The ^{12}C flux prior to inserting the PbF_2 target was generated by some low Cs^+ flux which could apparently not be cleaned completely. The altered $^{13}C^-/^{12}C^-$ ratio indicates a different sputter agent for the measurement part after inserting the PbF_2 target.

The base sputter ion flux of Cs^+ coming from remnant Cs in the ion source must be reduced as much as possible. This can be achieved by cleaning the ion source prior to the measurement and by lowering the ionizer power. On the other hand enough photon radiation has to be produced to initiate the self sputtering effects, so a compromise has to be found. For cesium targets mixed with PbF_2 Zhao et al. did not find very stable currents, also high source memory effect for the PbF_2-blanks were found with Blank/Cs-Target ≈ 0.25. The target containing of 2.5 mg Cs was mixed CsF:$PbF_2 = 1{:}6$ by weight (fig. 4.11) [46].

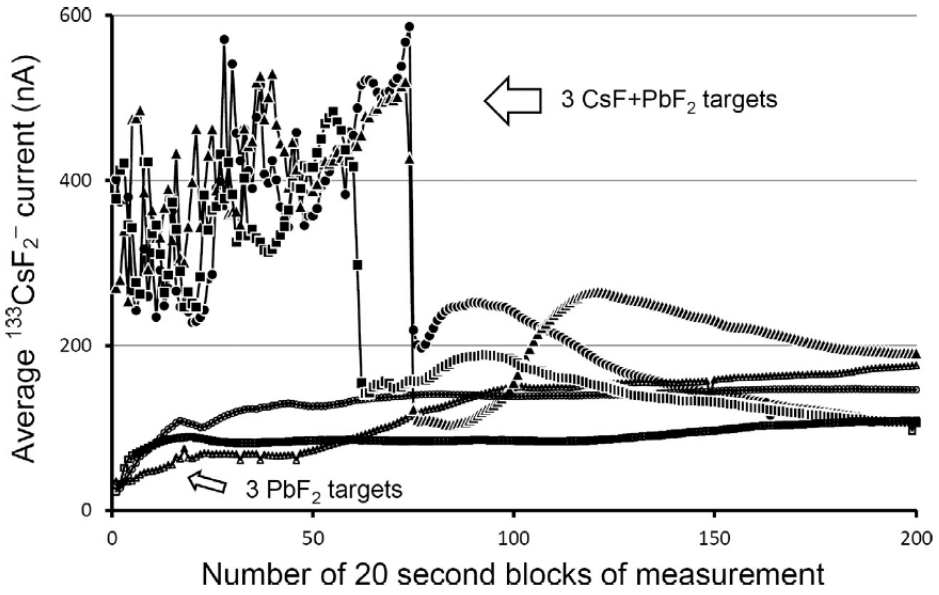

Figure 4.11: CsF+PbF_2-Targets were tested by Zhao et al. [46] at the Lalonde AMS laboratory and yielded an average ion current of 400 nA, while the Blank showed a very high ion current on mass 133 of 100 nA. [46]

Since PbF_2 has a relatively high vapor pressure of 0.28 Pa at 600 °C [63], a pure PbF_2-target evaporates quickly and does not yield a constant ion current output. For this reason metallic binders such as copper (4 nPa at 600 °C) or silver (4 μPa at 600 °C) [64] are used to improve thermal conductivity and lower the overall temperature of the target. Of course this dampens the fluorine mixing properties but should improve the stability of the ion current.

With similar effects of a self-sputtering sample seen at VERA, for the next beamtimes (following Cs1902a) the ion source, especially the ionizer was cleaned prior to the measurement to reduce the base sputter Cs^+ flux as much as possible. In addition to the mechanical cleaning, the source was rinsed with O_2. In normal AMS measurements we use graphite in Al holders as park cathode on position 0 of the sample wheel. The well studied output of C^- makes it easier to monitor source sensitive effects like ionizer poisoning or whether the sputter agent in the reservoir is used up. These graphite targets originate from old ^{14}C measurements and were therefore heavily sputtered by Cs^+. For Cs measurements it was avoided to put in those targets into the sample wheel.

Empty aluminum cathodes with only a copper pin in them were used as a park cathode instead. After the cleaning and prior to the beamtime the ionizer was outgased at 33 A ($\approx$ 250 W) to let the cesium which survived the mechanical and chemical cleaning move off the ionizer. Instead of the Rb reservoir an empty reservoir was installed. The so called "lineheater", the heated capillary which connects the, in our case, empty reservoir with the sample wheel volume was synchronously turned on with the ionizer.

For the beamtime Cs1902b, the first one without Rb sputtering, copper was added to some materials because of its low vapor pressure and high conductivity. Additionally, so called "offset blanks" containing no cesium were measured between the Cs samples to quantify the source memory effects.

Name	Material	Comment
Cs10	Cs_2SO_4+PbF_2	reference material $^{137}Cs/^{133}Cs = 1 \cdot 10^{-10}$
Blank	Cs_2SO_4+PbF_2	only Cs carrier + PbF_2
PbF_2	PbF_2	offset blank for monitoring source memory effect
CuinAl	empty	copper pin in Al cathode as park cathode
Cs10+Cu	Cs_2SO_4+PbF_2+Cu	reference material $^{137}Cs/^{133}Cs = 1 \cdot 10^{-10}$
Blank+Cu	Cs_2SO_4+PbF_2+Cu	only Cs carrier + PbF_2 + Cu
PbF_2+Cu	PbF_2+Cu	offset blank for monitoring source memory effect
Spike	BaF_2+Cs_2SO_4+PbF_2	Ba Spike for monitoring suppression

Table 4.3: Materials used during the first beamtime without rubidium sputtering (Cs1902b). Copper was added to some materials to increase the thermal conductivity.

The presented results of the measured isotopic ratios for the Cs10(+Cu) reference materials in fig. 4.12 and fig. 4.13 show a comparison between the two different sets of targets over a range of six measurements. The idea of increasing the thermal conductivity by adding copper is that more stable measurement conditions can be achieved and the cross contamination can be lowered. Only low reference materials were used ($^{137}Cs/^{133}Cs = 1 \cdot 10^{-10}$, which is two orders of magnitude lower than the maximum values in earlier beamtimes) to further decrease the source memory effects. The ionizer for these measurements was set to 32.5 A ($\approx$ 230 W) which gave a suitable ion current in the order of 100 nA but also increased the effect of cross contamination.

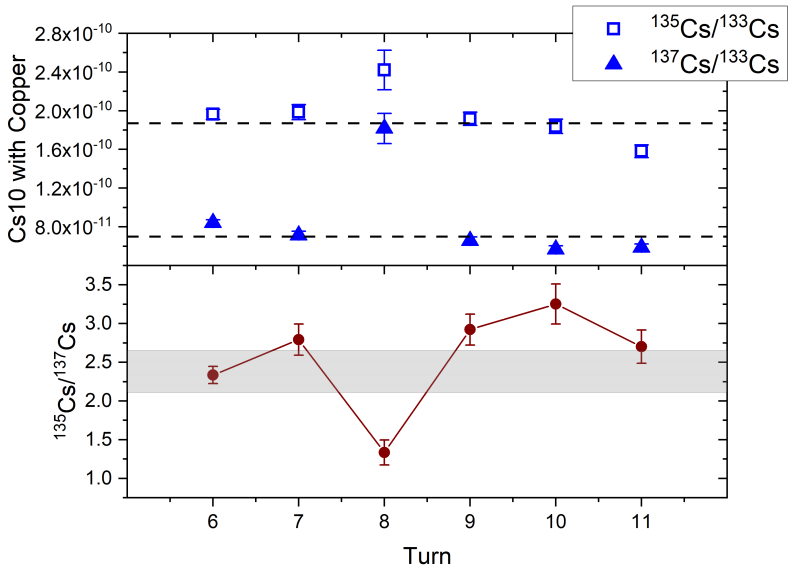

Figure 4.12: Six consecutive turns of a low reference material of $^{137}Cs/^{133}Cs = 1 \cdot 10^{-10}$ with copper (Cs10+Cu) yields a good first result for the $^{135}Cs/^{137}Cs$ ratio in our reference material.

Interestingly the two stable $^{135}Cs/^{137}Cs$-measurements of the samples mixed with copper and the ones without copper result in two different ratios of 2.38 $\pm$ 0.28 and 3.28 $\pm$ 0.10 (shaded areas in fig. 4.12 and fig. 4.13). If we neglect the deviating measurement during Turn 8, the value increases from 2.38 to 2.62 $\pm$ 0.15 for Cs10 with copper, still being significantly lower than for the other measurement. We can think of three potential explanations for the observed deviation between the Cu mixed and the pure Cs_2SO_4 samples: As we know from the experiments by Zhao et al. (fig. 4.10) the isotopic ratio can be altered by the sputtering process and the sputter agent. If the copper really has that major impact on this self sputtering process, it would be possible that this results in this observed slight difference between the $^{135}Cs/^{137}Cs$ ratios. While we have found it to be very difficult to obtain a stable $^{133}CsF_2^-$-beam over a long time span, it seems at the moment more realistic to justify these measured differences in the $^{135}Cs/^{137}Cs$ isotopic ratio with setup issues, as one of the two rare isotopes was not optimally tuned. The third possibility is the position of the wheel in the ion source, as

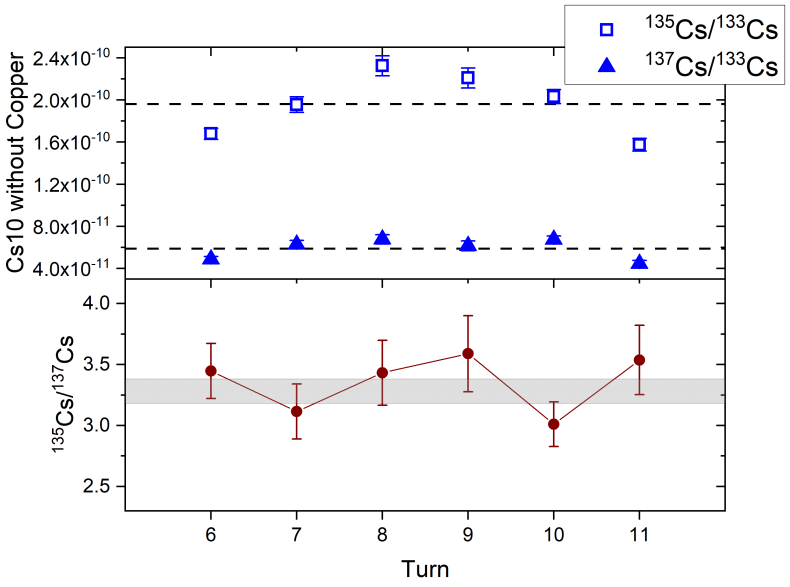

Figure 4.13: Measurements of a reference material without copper (Cs10). Both, ion current and isotopic ratio are stable throughout the six turns, however a difference in the $^{135}Cs/^{137}Cs$-ratio compared to the measurement shown in fig. 4.12 is seen.

these two compared samples had nearly opposite placements in the wheel (position 14 vs position 32 in a sample wheel with 40 positions) and the ion beam is only optimized for one initial position for tuning the mass 171 beam, which in this case was at position 5. The eccentricity of the wheel is the major problem of optimizing the reproducibility of the wheel position. So, normally the wheel should be centered at at least 4 positions, which lay opposite each other.

If we take the average of the values found for Cs10 and Cs10+Cu, we obtain an isotopic ratio of $^{135}Cs/^{137}Cs = 0.73 \pm 0.08$ decay corrected to 1964 which corresponds to a $3.5 \cdot 10^{13}\,cm^{-2}\,s^{-1}$ neutron flux according to eq. 2.1, which is in a realistic range if we consider fig. 2.3.

For better understanding of the source memory effect countrates on PbF_2-targets were compared between samples with copper and samples without copper. For a longer

sputter process a "cleaning" effect is seen (fig. 4.14). As we expected, the countrates on the targets mixed with copper were significantly smaller than on the targets without copper, which suggests a reduction of the source memory effect.

Interestingly, the isotopic ratio $^{135}Cs/^{133}Cs$ for the PbF_2 targets is higher by a factor 2 than on the blank containing cesium. This is a strong indicator that the strength of the source memory effect is dependent on the amount of PbF_2 in a sample, which leads us to a dilemma since we need much fluorine in the source to operate it at a high CsF_2^- output.

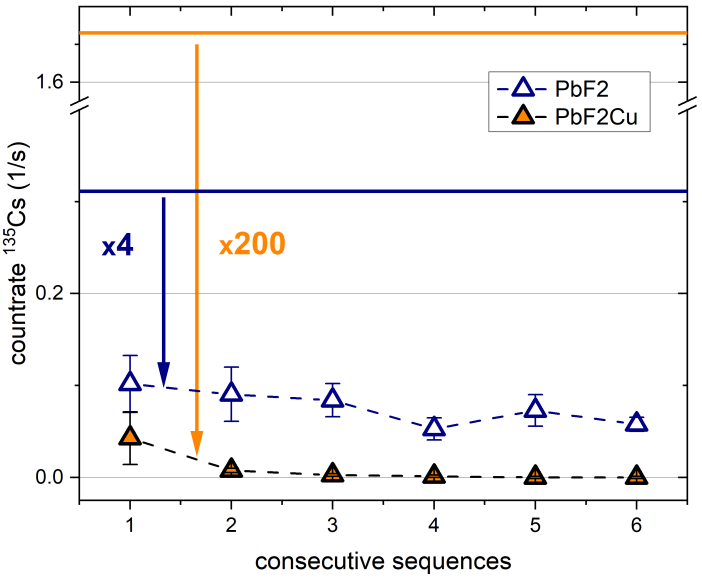

Figure 4.14: ^{135}Cs countrates for six consecutive sequences ($\widehat{=}$ 2 Runs) on targets not containing cesium: PbF_2 and PbF_2+Cu. The countrates are averaged from several targets. Each sequence was measured 160 s with about 30 s in between. The countrates on the reference materials measured right before the non-Cs targets were 1.76/s (orange line) for the PbF_2+Cu-target and 0.31/s (blue line) for the PbF_2-target. This gives a source memory effect from reference material to the non-Cs targets of 25 % for the materials not mixed with copper and only of 0.5 % for the materials mixed with copper.

For examining the sputter agent in the measurements without Rb reservoir and quantizing the qualitative effect of cross contamination reduction seen in fig. 4.14, the deposits on the sample wheel where investigated by PIXE at VERA.

4.3.4 PIXE measurements of sample wheel

PIXE stands for **P**roton **I**nduced **X**-ray **E**mission and is a precise and non-destructive method for elemental analysis used in archaeology, geology and by conservators. A proton beam of few MeV is produced in the accelerator and focused on the target. Inner shells of the bombarded atoms will be ionized, which causes outer electrons to fill this gap and release a photon with, as only certain transition energies are allowed, definite wavelength. These x-ray emissions get detected by a SiLi-detector and unambiguous elemental analysis is possible.

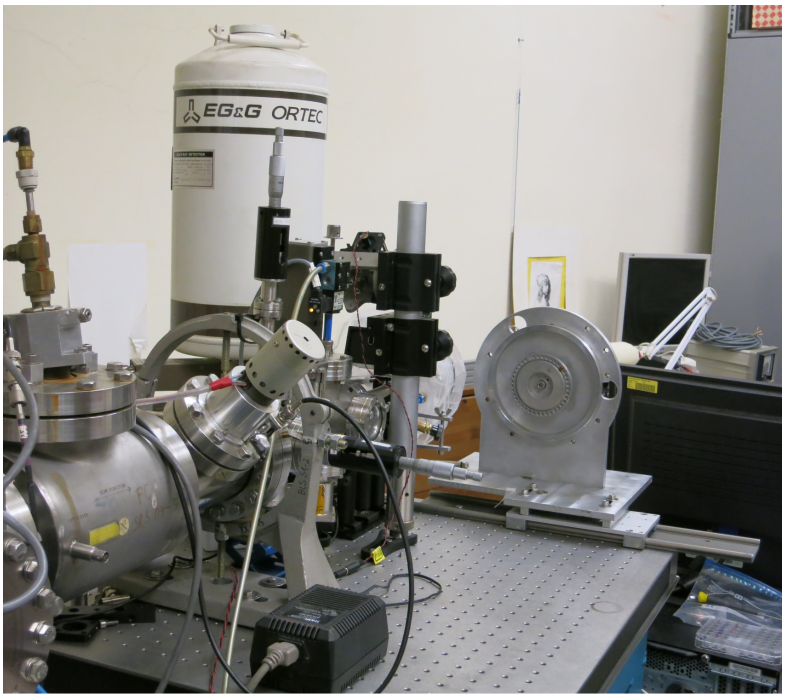

Figure 4.15: Picture of the current PIXE structure at VERA. One can see the sample wheel, which is movable into a helium surrounding to suppress the prominent argon peak from air. On the left the beamline with slits, beam profile monitor and ZnS-shield for orientating the proton beam can be seen.

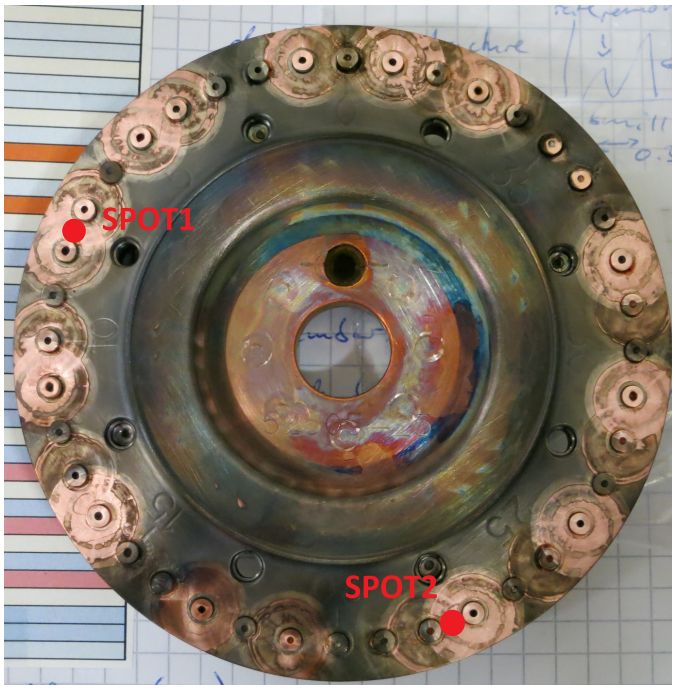

Figure 4.16: Sample wheel measured with PIXE: Two spots were examined and the difference in sputtered Cs-material on the surface of the wheel was calculated.

The PIXE beamline at VERA was originally installed in 2004 with the purpose of measuring renaissance silverpoint drawings of Albrecht Dürer [65]. Today it is mostly used for monitoring chemical sample preparation as it can quantify large stable isotopic abundances precisely [66]. In our case we wanted to measure what kind of elements were deposited on the surface of our sample wheel, as it could bring some information about the sputter agent and the severity of the cross contamination. For this purpose 3 MeV protons were produced using a TiH-sample in the ion source and two spots of our sample wheel were examined. One spot which lies between a Blank and a PbF_2-target and the other spot lies between a Blank mixed with copper and and a PbF_2-target mixed with copper (see fig. 4.16). The results are shown in 4.17. Both spectra were measured 650 s and the proton rate was determined by a gas ionization chamber, located just before the PIXE beamline, to be about 300/s before and after the measurement. In general proton countrates between 300 and 1000 per second were observed during other PIXE measurements [67].

A strong indicator for the comparability of the two measurements are the Kα and the Kβ-Peaks of copper, which origin mainly from the copper wheel. The additionally mixed in copper is thought to make no difference in these scales ($> 10^4$ counts in 650 s). In fig. 4.17 one can see, that the cesium peaks and the sulfur peak are much higher for the spot between the cathodes without copper. We should take into account that both samples were not equally long measured and also gave not equal ion current output. For that reason we normalize to the charge output Q of each blank, which turned out to be similar ($\Delta Q/Q < 10\%$). As we do not monitor the ion current in the faraday cup right after the ion source, we use the high-energy side ion current for calculation and assume direct proportionality between those two values. Although the ion cooler and accelerator transmission are ion current dependent, the output of these two blanks should differ sufficiently small, so that we still get an estimation of deposition of material on the sample wheel.

	Spot 1	Spot 2
Counts in 650 s	47620 ± 470	27980 ± 530
Sputtered charge from Blank [C]	$9.849 \cdot 10^{-5}$	$9.120 \cdot 10^{-5}$
Normalized Cs-Peaks [Counts/(C · s)]	$7.44 \cdot 10^6$	$4.72 \cdot 10^6$

One can see that the additional mixed copper indeed results in a suppression of cross contamination by a factor $7.44/4.72 = 1.58$. The same calculation can be done for the sulfur peak. There the reduction factor was found to be 2.12, which is 34 % higher than the value found for the Cs peaks. Although these two factors should be equal, uncertainties in the range of the relative difference between those values are reasonable. Therefore, this confirms the qualitative effect we saw in the PbF_2+Cu countrates: The additionally mixed in copper improves the thermal conductivity and lowers the overall temperature of the target. This dampens the fluorine mixing and inhibits the ion source memory effect.

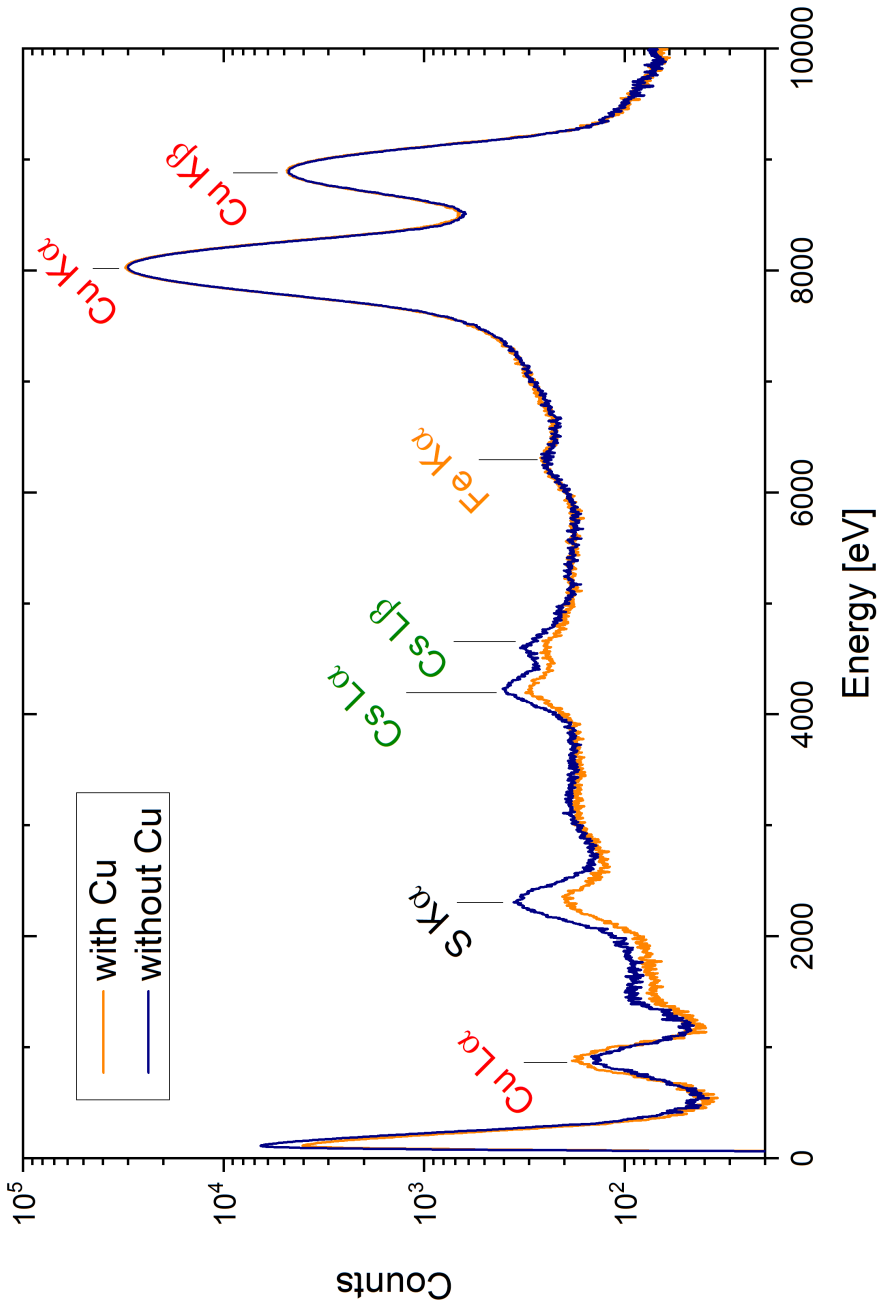

Figure 4.17: Spectra of both measurements, each 650 s, on two spots between a blank and a PbF_2-target each. At one spot the two flanking targets where mixed with copper, at the other not. A difference in sputtered material deposition on the wheel is clearly visible but has to be normalized to the sputtered charge to make a quantitative comparison.

4.4 Suppression of m/q interferences

As explained in chapter 2.2, ions in AMS are selected by their mass over charge ratio. So called m/q interferences can therefore not be distinguished from the isotope of interest by a basic mass spectrometer. However, as far as these interferences are not too intense, the ions can be separated by their stopping power due to their different proton number. For $^{135}Cs^{+3}$, there are two m/q interferences: $^{90}Zr^{2+}$ and $^{45}Sc^{1+}$. For ^{137}Cs no m/q interferences are possible. In fig. 4.18 two measurements on a barium spiked material and a reference material with laser off and on, respectively, are shown. One can clearly identify the m/q interferences and separate it from cesium. Barium can not be distinguished from cesium events in the detector at the terminal voltage we operate.

The detection efficiency is assumed to be 100 %. With the high suppression factors for barium, we assume that only cesium ions are counted in the region of interest if the laser is turned on and that mainly barium is detected if the laser is turned off. This is a good approximation due to the overwhelming amount of stable barium which leads to countrates of $10^4/s$, while for cesium the countrates on high reference materials are $10/s$ at maximum.

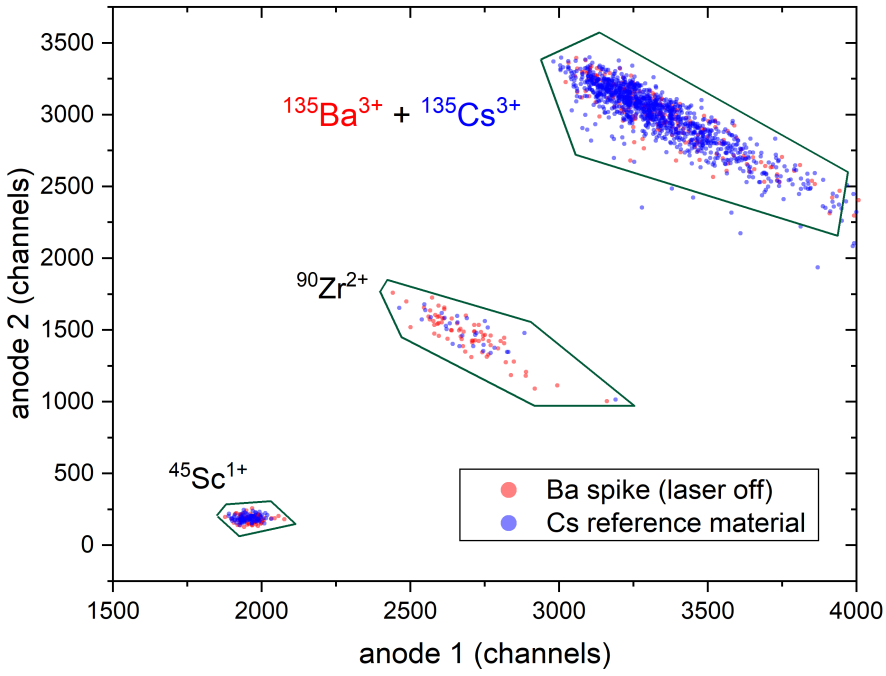

Figure 4.18: M/q-interferences are well separated from ^{135}Cs in the gas-filled ionization chamber. For the barium spike there is no separation of the $^{135}Ba^{3+}$ events on the two anodes from the $^{135}Cs^{3+}$ counts

4.5 Isobar suppression with ILIAMS

As we cannot differentiate between Ba^{3+} and Cs^{3+} in the detector (see fig. 3.2 and 4.18) we have to find other ways to monitor the barium suppression throughout a measurement. It is immanently important to suppress barium completely via photodetachment, so we can assume that every count in the detector is from cesium or one of its m/q-interferences, which are separable in the detector. For this reason we monitor mass 134 and 136 during the measurement, where no cesium should be seen. So all counts on these masses show us an insufficient suppression behaviour. On mass 136 the countrate is unexpectedly high. It stems from CeF_2^-, which has a very small electron affinity and is completely destroyed at transmitted laser powers of 0.1 W or even lower. CeF_2^- is therefore no problem while monitoring the barium suppression.

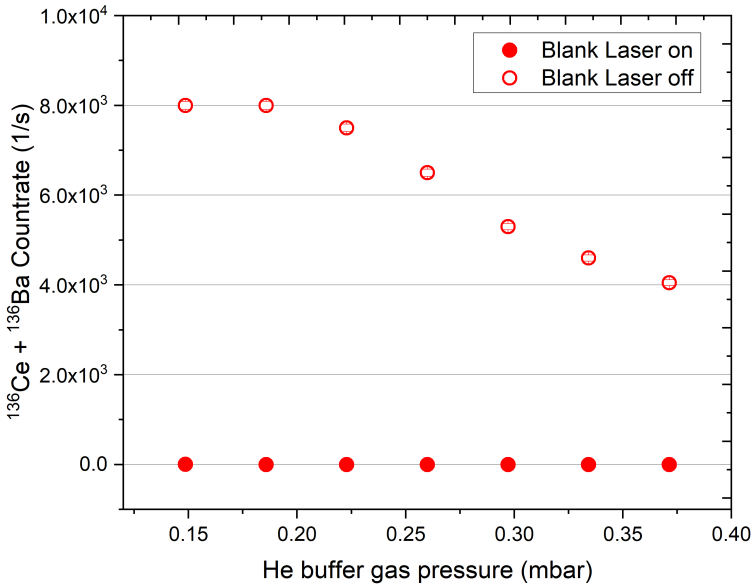

Figure 4.19: Cooler pressure dependent countrate for mass 136. It is not a priori clear in which shares barium and cerium divide but both are completely suppressed by the laser. For this measurement the laser was operated to transmit 10 W power. The extracted molecules from the ion source were CeF_2^- and BaF_2^-.

For the reference materials and the blanks, it is expected that the cesium stays unaffected by the buffer gas pressure and the laser. For the relevant masses 135 and 137, no cerium interference is possible, since cerium has stable isotopes only on masses 136, 138, 140 and 142.

The goal of the buffer gas scans is to determine the buffer gas pressure at which the barium gets suppressed. In fig. 4.20 one can see both the suppression of barium by one order of magnitude by kinetic reactions with the gas by raising the buffer gas pressure from 0.15 mbar to 0.37 mbar and the additional four orders of magnitude suppression done by turning on the laser. Again the laser was operated to transmit 10 W power trough the ion cooler. At mass 136 (fig. 4.19), we observe no counts at all for the measurement with the laser turned on. At mass 137 (fig. 4.20) the blank countrate is non-zero, even with the laser turned on, which could be due to cross contamination

of ^{137}Cs. The drop in this countrate with rising buffer gas pressure could be more of a chronological effect of the measurement, rather than one of rising pressure. This should be checked by a repeated measurement scanning the buffer gas pressure in both directions. In this measurement the cesium stays completely unaffected by the buffer gas pressure over a wide range.

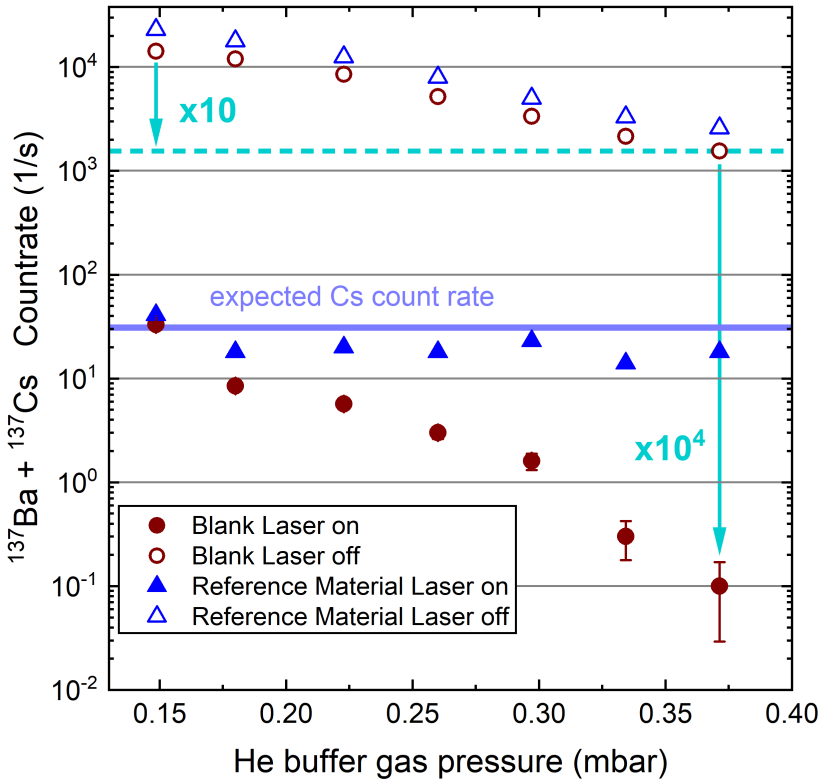

Figure 4.20: Cooler pressure dependent countrate for mass 137

For mass 135 this result was only partly reproducible. While the overall suppression is the same, a stronger reduction of the countrate by raising the buffer gas is seen (fig. 4.21). This can only be explained by setup issues, since it affects both blank and

reference material and a stable measurement environment at higher buffer gas pressures was not given anymore. Theoretically, there should be no difference in behavior in the ion cooler between the two masses.

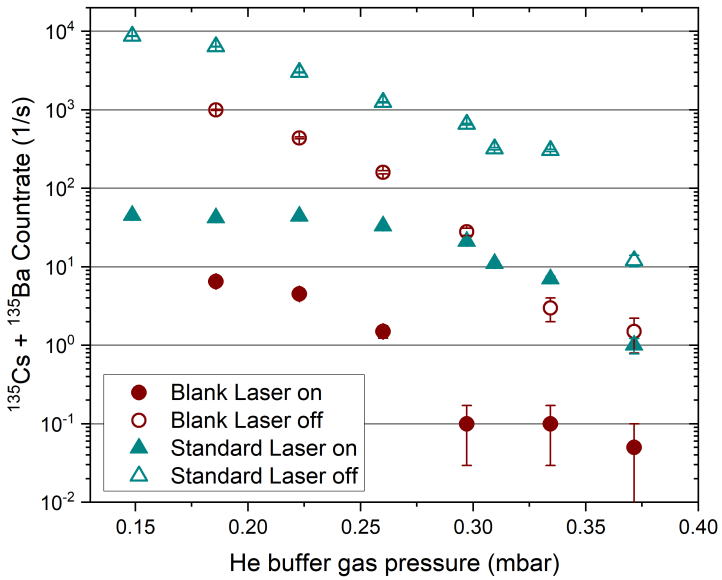

Figure 4.21: Cooler pressure dependent countrate for mass 135

In general the barium counts decrease exponentially with the rising buffer gas by kinetical interactions. On the relevant masses 135 and 137 for high buffer gases only partly reproducible results could be obtained. The complete suppression of barium and cerium on mass 136 with usage of the laser leads to the suspicion that the countrate on the blank at high gas pressures stems from cross contamination.

Measurements on the Ba spike without the laser were done to give an estimation of the overall suppression of barium which can be achieved by VERA. For this reason two measurements were done on mass 136 and 134, where only mass 136 suffers from Ce interference. With the known natural abundances of $^{136,134}Ba$ and the measurement of the total number of counts on these masses, one can estimate the share of ^{136}Ba counts. For 0.15 mbar of buffer gas pressure we found 720 counts per second on mass 134,

with the laser turned off. On the same target a few minutes afterwards, we found 8000 counts per second on mass 136. One can calculate from the natural $^{136}\mathrm{Ba}/^{134}\mathrm{Ba} = 3.25$ that $\approx 30\%$ of the counts on mass 136 are barium counts.

So we get an isotopic ratio of $^{136}\mathrm{Ba}/^{133}\mathrm{Cs} = 1.5 \cdot 10^{-6}$ on the spike with turned off laser, while with the laser turned on the relatively low ^{133}Cs ion current output limits us to blank level of $^{136}\mathrm{Ba}/^{133}\mathrm{Cs} < 3.5 \cdot 10^{-12}$. The cesium stays unaffected from the overlapping laser beam, but collisions with the buffer gas lead to losses of ion current. At the moment we reach transmissions of about 25 – 30 % through the ion cooler for ^{133}Cs. This gives a suppression factor of $> 10^5$ by ILIAMS. As there is no suppression possible in the gas filled ionization chamber and Kasberger et al. found a suppression factor of ≈ 12 in the ion source in earlier studies [41], an overall suppression factor of $> 10^6$ was achieved at VERA.

4.6 Reference materials with determined $^{135}Cs/^{137}Cs$ ratio

In this section a short overview of reference materials with determined $^{135}Cs/^{137}Cs$ ratio by other techniques will be given. Also first test runs on these materials at VERA were performed. The investigated reference materials should show the isotopic signature of global fallout and the Chernobyl nuclear accident. The $^{135}Cs/^{137}Cs$ ratio for the latter is already well studied by different groups with a consensus value of 0.297 ± 0.001 [14] [68] [69].

4.6.1 Chemical treatment

In-house reference material

For the in-house reference material the with HNO_3 diluted 2 Bq/ml Amersham solution was mixed with a solution made from the Cs_2SO_4 mixed with milli-Q water in the right amounts to obtain the desired $^{137}Cs/^{133}Cs$ ratio. This solution gets dried at about 70 °C for several hours on a heating plate. To this dried powder PbF_2 gets added in Cs:F = 1:4 ratio (atomic) which can be calculated to Cs_2SO_4:PbF_2 = 1:2.8 (weight). To this powder again a few ml milli-Q are added and again dried at 70 °C. Note that PbF_2 is defined as "very slightly soluble" with a low solubility of 0.65 g/l [70]. On the other hand the fluorine is very mobile in the ion source, so no homogeneity problems should occur. This powder then gets mixed with metallic copper in Cs:Cu = 1:1 ratio (atomic). It was found to be sufficient to mix the copper just with the spatula into the material.

IAEA reference material

For the IAEA reference materials the chemical treatment was done by our colleague Maki Honda. The recipe for extracting cesium from the material is shown in fig. 4.22 [71]. In the final step the solution is mixed with 1 % H_2SO_4 and dried up. The mixing ratio of Cs:F:Cu = 1:4:1 (atomic) is the same as for the in-house reference material

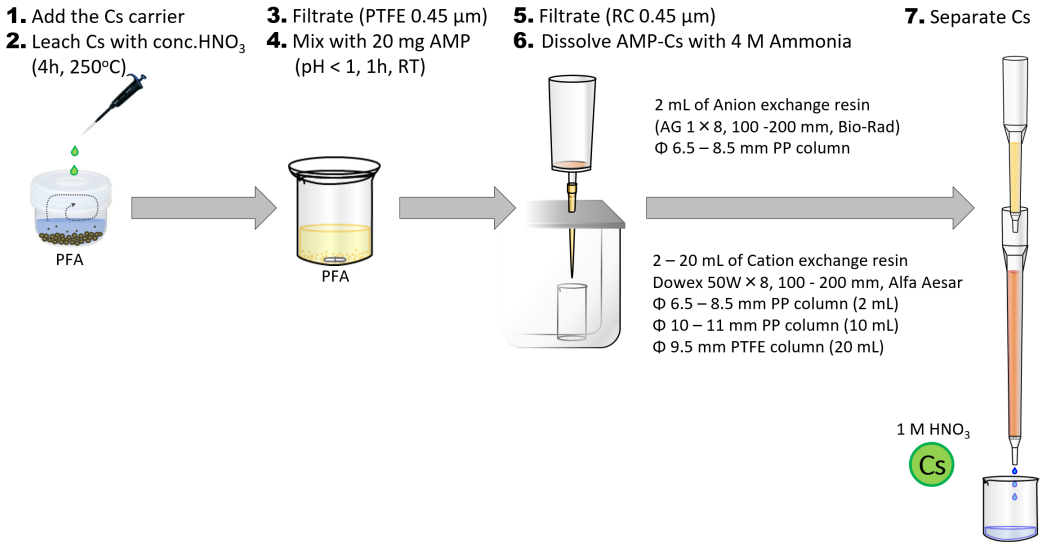

Figure 4.22: Chemical extraction of cesium for the IAEA reference materials [71]

4.6.2 IAEA 372

The grass for this reference material was obtained in 1990 from Kiev, Ukraine. Its intended use is for calibration due to its high ^{40}K (1060 $\pm$ 56 Bq/kg) and ^{137}Cs (11320 $\pm$ 360 Bq/kg) activity [72] [73]. We aim to detect the $^{135}Cs/^{137}Cs$-signature of the Chernobyl nuclear accident in this sample. Bu et al. obtained a value of $^{135}Cs/^{137}Cs = 0.612 \pm 0.008$ (decay corrected to January 1st 2018) with TIMS [14]. As one can see in 4.23, our measurement series in this beamtime suffered from stability issues. Problems with the ion source did not allow us to gain data in a stable measurement environment[1].

The ^{137}Cs concentration, calculated with measured $^{137}Cs/^{133}Cs$ ratios, was found to be measured more than one order of magnitude lower than expected from the activity given in the data sheet, which is another strong indicator that this measurement series has to be done again to get more reliable data.

[1] Due to our measurement method of sputtering without any oven, the the ion current output is very sensitive to the wheel position. The wheel has to be centered in the focus of the ionizer. Between the ionizer and the sample wheel a tantalum shield is located, which was at that time (Cs1908) slightly bent, so it was not possible to rotate the sample wheel in the optimum position without hitting this shield. The wheel had to be backed up a few millimeters before rotating and then had to be put back in optimum position. Unfortunately, this procedure resulted in unstable measurement conditions.

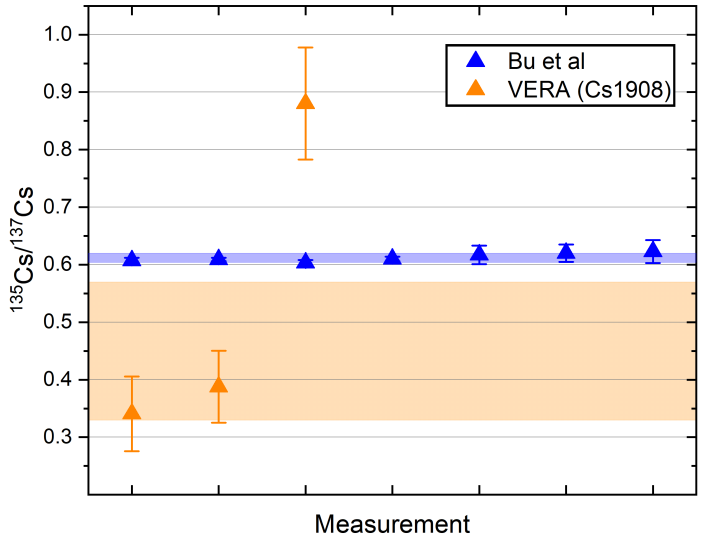

Figure 4.23: Comparison between measurements on IAEA372 with TIMS by Bu et al. [14] and the measurements done at VERA. The shaded areas depict the uncertainty of the mean value of all measurements. All values are decay corrected to January 1st 2018

4.6.3 IAEA 447

The moss-soil for this reference material was collected in an abandoned marble mine in the north-west of Hungary in 2007. The undisturbed moss growth is ideal to use it as a memory record for the radioactive fallout (^{137}Cs massic activity: 425 $\pm$ 10 Bq/kg) [74] [75]. Unfortunately we could not measure any radiocesium in the material. A control measurement after the AMS measurement was performed with the HPGe detector on the sputtered target. It showed no gamma activity (see fig. 4.24) although one could have expected that 0.3 Bq are present in the processed sample. This indicates that the Cs was lost in the chemical processing. Yang et al. [4] found a $^{135}Cs/^{137}Cs$ ratio of 1.44 $\pm$ 0.23 decay corrected to November 15th 2009, which is the reference date in the IAEA 447 reference sheet.

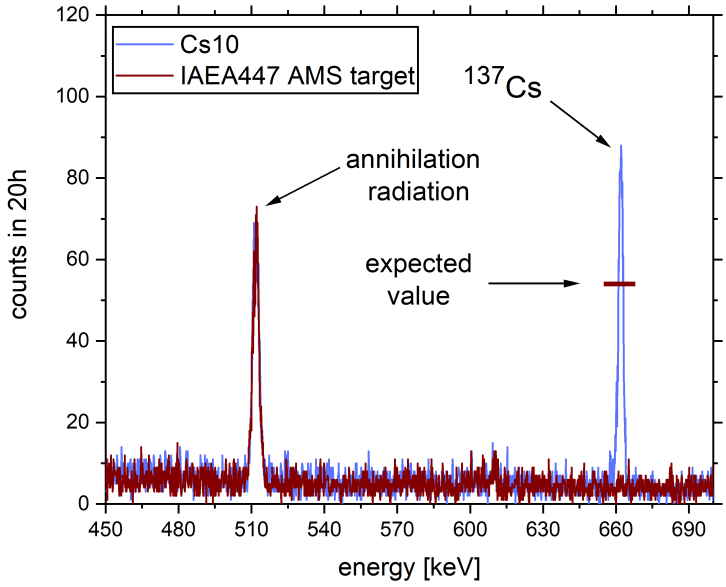

Figure 4.24: Gamma measurements performed with the HPGe detector to control the AMS measurements. As a reference to IAEA 477 a in-house reference material (Cs10), with similar activity was tested too. The expected value for IAEA 447 at 662 keV was calculated for a 8 mg Cs10 target (2 mg Cs_2SO_4, 6 mg PbF_2) and 1 mg of added Cs carrier to the IAEA 447 sample. Further, no losses during the sample press procedure for IAEA 447 are assumed. Still we should see a countrate significantly above the background.

4.6.4 Other reference materials to investigate

In this table a brief summary of all reference materials is given, in which the $^{135}Cs/^{137}Cs$ ratio was already determined.

The reference materials with the Chernobyl signature are already well studied with uncertainties in the range of less than one percent. The higher uncertainties for the two NIST materials derive presumably from the much lower activity in these samples (29 and 14 Bq/kg) despite being measured by the same group with the same technique. The measurements performed by ICP MS have much larger uncertainties with 16 % and 31 %.

Name	$^{135}Cs/^{137}Cs$	Reference	Method
IAEA 372	0.296 ± 0.004^a	[14]	TIMS
IAEA 330	0.297 ± 0.001^a	[14]	TIMS
IAEA 375	0.30 ± 0.01^a	[68]	TIMS
IAEA 156	0.299 ± 0.003^a	[69]	TIMS
IAEA 447	1.44 ± 0.23^b	[4]	ICP-MS/MS
IAEA 385	0.52 ± 0.16^b	[4]	ICP-MS/MS
NIST 4353a	2.81 ± 0.19^c	[14]	TIMS
NIST 4354	3.16 ± 0.13^c	[14]	TIMS

Table 4.4: ^{a}values are decay corrected to April 26$^{\text{th}}$ 1986, ^{b}values are decay corrected to reference date given in their respective reference sheet, ^{c}values are decay corrected to January 1$^{\text{st}}$ 2018

5 Conclusion & Outlook

^{135}Cs was successfully measured with respect to its sister isotope ^{137}Cs and the stable ^{133}Cs. By using the new approach of a self-sputtering ion source without any external sputter agent, high CsF_2^- currents in the range from 100 nA to 1 μA from a Cs_2SO_4+PbF_2+Cu matrix were extracted. Further, the blank value was decreased by almost two orders of magnitude with respect to the method of rubidium sputtering. Still the anticipated goal of an abundance sensitivity of $^{135}Cs/Cs \approx 10^{-14}$, which is necessary for measuring environmental samples, was not yet achieved. Problems with cross contamination from high reference materials and source memory effects are major challenges for successful measurement of the radioactive Cs isotopes. Nevertheless, the suppression of the interfering isobars ^{135}Ba and ^{137}Ba by laser photodetachment was in the order of 10^5 on top of the suppression in the ion source by extracting F_2^--fluorides. This makes the barium interference nearly irrelevant for practical applications.

In the near future, measurements on reference materials with already determined $^{135}Cs/^{137}Cs$ ratio will be investigated and compared with other mass spectrometric methods. For even better suppression factors tests with different buffer gases such as hydrogen will be made. Also, the ionization efficiency for CsF_2^- was not yet investigated, which is a big factor for making the measurement procedure as effective as possible.

The final aim is to make ^{135}Cs a routine measurement isotope at VERA. At the moment ^{26}Al and ^{36}Cl are already measured routinely with ILIAMS. The new isotopes ^{135}Cs and ^{90}Sr are to follow in foreseeable future.

Bibliography

[1] MacDonald, C. M. ; Cornett, R. J. ; Charles, C. R. J. ; Zhao, X. L. ; Kieser, W. E.: Measurement of the ^{135}Cs half-life with accelerator mass spectrometry and inductively coupled plasma mass spectrometry. In: *Phys. Rev. C* 93 (2016), Jan, 014310. https://link.aps.org/doi/10.1103/PhysRevC.93.014310

[2] Nuclear Data Center - Japan Atomic Energy Agency, Nuclide Information Sheet 135Cs. https://wwwndc.jaea.go.jp/cgi-bin/nuclinfo2014?55,135

[3] Lachner, Johannes ; Kasberger, Magdalena ; Martschini, Martin ; Priller, Alfred ; Steier, Peter ; Golser, Robin: Developments towards detection of 135Cs at VERA. In: *Nuclear Instruments and Methods in Physics Research Section B: Beam Interactions with Materials and Atoms* 361 (2015), 440 - 444. https://doi.org/10.1016/j.nimb.2015.01.032. – ISSN 0168–583X

[4] Yang, Guosheng ; Tazoe, Hirofumi ; Yamada, Masatoshi: Rapid determination of 135Cs and precise 135Cs/137Cs atomic ratio in environmental samples by single-column chromatography coupled to triple-quadrupole inductively coupled plasma-mass spectrometry. In: *Analytica Chimica Acta* 908 (2016), 177 - 184. https://doi.org/10.1016/j.aca.2015.12.041. – ISSN 0003–2670

[5] Taylor, V.F. ; Evans, R.D. ; Cornett, R.J.: Preliminary evaluation of 135Cs/137Cs as a forensic tool for identifying source of radioactive contamination. In: *Journal of Environmental Radioactivity* 99 (2008), Nr. 1, 109 - 118. https://doi.org/10.1016/j.jenvrad.2007.07.006. – ISSN 0265–931X

[6] Forstner, Oliver ; Andersson, Pontus ; Hanstorp, Dag ; Lahner, Johannes ; Martschini, Martin ; Pitters, Johanna ; Priller, Alfred ;

Steier, Peter ; Golser, Robin: The ILIAS project for selective isobar suppression by laser photodetachment. In: *Nuclear Instruments and Methods in Physics Research Section B: Beam Interactions with Materials and Atoms* 361 (2015), 217 - 221. http://www.sciencedirect.com/science/article/pii/S0168583X15003596. – ISSN 0168–583X

[7] Kinsey, R. R.: The NUDAT/PCNUDAT Program for Nuclear Data. https://www.nndc.bnl.gov/nudat2/

[8] Chino, Masamichi ; Terada, Hiroaki ; Nagai, Haruyasu ; Katata, Genki ; Mikami, Satoshi ; Torii, Tatsuo ; Saito, Kimiaki ; Nishizawa, Yukiyasu: Utilization of 134Cs/137Cs in the environment to identify the reactor units that caused atmospheric releases during the Fukushima Daiichi accident. In: *Scientific Reports* 6 (2016), 2045-2322. https://doi.org/10.1038/srep31376. – ISSN 2045–2322

[9] Delmore, James E. ; Snyder, Darin C. ; Tranter, Troy ; Mann, Nick R.: Cesium isotope ratios as indicators of nuclear power plant operations. In: *Journal of Environmental Radioactivity* 102 (2011), Nr. 11, 1008 - 1011. http://www.sciencedirect.com/science/article/pii/S0265931X11001561. – ISSN 0265–931X

[10] Pibida, L. ; McMahon, C.A. ; Bushaw, B.A.: Laser resonance ionization mass spectrometry measurements of cesium in nuclear burn-up and sediment samples. In: *Applied Radiation and Isotopes* 60 (2004), Nr. 2, 567 - 570. http://dx.doi.org/https://doi.org/10.1016/j.apradiso.2003.11.082. – DOI https://doi.org/10.1016/j.apradiso.2003.11.082. – ISSN 0969–8043

[11] Snow, Mathew S. ; Snyder, Darin C. ; Clark, Sue B. ; Kelley, Morgan ; Delmore, James E.: 137Cs Activities and 135Cs/137Cs Isotopic Ratios from Soils at Idaho National Laboratory: A Case Study for Contaminant Source Attribution in the Vicinity of Nuclear Facilities. In: *Environmental Science & Technology* 49 (2015), Nr. 5, 2741-2748. https://doi.org/10.1021/es5058852

[12] Lee, Typhoon ; Teh-Lung, Ku ; Hsiao-Ling, Lu ; Ju-Chin, Chen: First detection of fallout Cs-135 and potential applications of 137Cs135Cs ratios. In:

Geochimica et Cosmochimica Acta 57 (1993), Nr. 14, 3493 - 3497. http://www.sciencedirect.com/science/article/pii/001670379390555B. – ISSN 0016–7037

[13] Snyder, Darin C. ; Delmore, James E. ; Tranter, Troy ; Mann, Nick R. ; Abbott, Michael L. ; Olson, John E.: Radioactive cesium isotope ratios as a tool for determining dispersal and re-dispersal mechanisms downwind from the Nevada Nuclear Security Site. In: *Journal of Environmental Radioactivity* 110 (2012), 46 - 52. http://www.sciencedirect.com/science/article/pii/S0265931X12000306. – ISSN 0265–931X

[14] Bu, Wenting ; Tang, Lei ; Liu, Xuemei ; Wang, Zhongtang ; Fukuda, Miho ; Zheng, Jian ; Aono, Tatsuo ; Hu, Sheng ; Wang, Xiaolin: Ultra-trace determination of the 135Cs/137Cs isotopic ratio by thermal ionization mass spectrometry with application to Fukushima marine sediment samples. In: *J. Anal. At. Spectrom.* 34 (2019), 301-309. http://dx.doi.org/10.1039/C8JA00380G

[15] E., Lewis E.: *Fundamentals of Nuclear Reactor Physics*. Bd. 1. 2008 https://www.elsevier.com/books/fundamentals-of-nuclear-reactor-physics/lewis/978-0-12-370631-7. – ISBN 9780080560434

[16] Shibata, K. ; Iwamoto, O. ; Nakagawa, T. ; Iwamoto, N. ; Ichihara, A. ; Kunieda, S. ; Chiba, S. ; Furutaka, K. ; Otuka, N. ; Ohsawa, T. ; Murata, T. ; Matsunobu, H. ; Zukeran, A. ; Kamada, S. ; Katakura, J.: JENDL-4.0: A New Library for Nuclear Science and Engineering. In: *J. Nucl. Sci. Technol.* 48 (2011), S. 1–30

[17] Yaroshevsky, A. A.: Abundances of chemical elements in the Earth's crust. In: *Geochemistry International* 44 (2006), Jan, Nr. 1, 48–55. https://doi.org/10.1134/S001670290601006X. – ISSN 1556–1968

[18] Katakura, J.: JENDL FP Decay Data File 2011 and Fission Yields Data File 2011. (2011). https://wwwndc.jaea.go.jp/cgi-bin/FPYfig

[19] Katakura, J. ; Minato, F. ; Ohgama, K.: Revision of the JENDL FP Fission Yield Data. (2016). https://wwwndc.jaea.go.jp/cgi-bin/FPYfig

[20] JAEA Nuclear Data Center - Nuclide Information. https://wwwndc.jaea.go.jp/NuC/index.html

[21] Chao, Jiunn-Hsing ; Tseng, Chia-Lian: Determination of 135Cs by neutron activation analysis. In: *Nuclear Instruments and Methods in Physics Research Section A: Accelerators, Spectrometers, Detectors and Associated Equipment* 372 (1996), Nr. 1, 275 - 279. http://www.sciencedirect.com/science/article/pii/0168900295012966. – ISSN 0168–9002

[22] Nuclear Data Center - Japan Atomic Energy Agency, Nuclide Information Sheet 137Cs. https://wwwndc.jaea.go.jp/cgi-bin/nuclinfo2014?55,137

[23] England, T.R. ; Rider, B.F.: Evaluation and compilation of fission product yields 1993. (1995), 12. http://dx.doi.org/10.2172/10103145. – DOI 10.2172/10103145

[24] Shultis, J. K.: *Fundamentals of nuclear science and engineering*. Third edition, version date: 20160804. Boca Raton, FL : CRC Press, 2017. – ISBN 9781498769297

[25] Bratsch, Steven G. ; Lagowski, J.J.: Predicted stabilities of monatomic anions in water and liquid ammonia at 298.15 K. In: *Polyhedron* 5 (1986), Nr. 11, 1763 - 1770. http://www.sciencedirect.com/science/article/pii/S0277538700848548. – ISSN 0277–5387

[26] Jacob, S.A.W. ; Suter, M. ; Synal, H.-A: Ion beam interaction with stripper gas – Key for AMS at sub MeV. In: *Nuclear Instruments and Methods in Physics Research Section B: Beam Interactions with Materials and Atoms* 172 (2000), 10, S. 235–241. http://dx.doi.org/10.1016/S0168-583X(00)00205-6. – DOI 10.1016/S0168–583X(00)00205–6

[27] Synal, Hans-Arno: Developments in accelerator mass spectrometry. In: *International Journal of Mass Spectrometry* 349-350 (2013), 192 - 202. http://www.sciencedirect.com/science/article/pii/S1387380613001772. – ISSN 1387–3806

[28] Lachner, Johannes ; Christl, Marcus ; Vockenhuber, Christof ; Synal, Hans-Arno: Detection of UH3+ and ThH3+ molecules and 236U background studies with low-energy AMS. In: *Nuclear Instruments and Methods in Physics Research Section B: Beam Interactions with Materials and Atoms* 294 (2013), 364 - 368. http://www.sciencedirect.com/science/article/pii/S0168583X12000997. – ISSN 0168–583X

[29] Kutschera, Walter: Accelerator mass spectrometry: state of the art and perspectives. In: *Advances in Physics: X* 1 (2016), Nr. 4, 570-595. https://doi.org/10.1080/23746149.2016.1224603

[30] Hain, Karin ; Deneva, Boyana ; Faestermann, Thomas ; Fimiani, Leticia ; Gómez-Guzmán, José M. ; Koll, Dominik ; Korschinek, Gunther ; Ludwig, Peter ; Sergeyeva, Victoria ; Thiollay, Nicolas: AMS of 93Zr: Passive absorber versus gas-filled magnet. In: *Nuclear Instruments and Methods in Physics Research Section B: Beam Interactions with Materials and Atoms* 423 (2018), 42 - 48. http://www.sciencedirect.com/science/article/pii/S0168583X18301629. – ISSN 0168–583X

[31] Herb, R.G.: Pelletron accelerators for very high voltage. In: *Nuclear Instruments and Methods* 122 (1974), 267 - 276. http://www.sciencedirect.com/science/article/pii/0029554X7490487X. – ISSN 0029–554X

[32] Kutschera, W. ; Collon, P. ; Friedmann, H. ; Golser, R. ; Hille, P. ; Priller, A. ; Rom, W. ; Steier, P. ; Tagesen, S. ; Wallner, A. ; Wild, E. ; Winkler, G.: VERA: A new AMS facility in Vienna. In: *Nuclear Instruments and Methods in Physics Research Section B: Beam Interactions with Materials and Atoms* 123 (1997), Nr. 1, 47 - 50. http://www.sciencedirect.com/science/article/pii/S0168583X96007823. – ISSN 0168–583X

[33] Martschini, Martin ; Hanstorp, Dag ; Lachner, Johannes ; Marek, Christoph ; Priller, Alfred ; Steier, Peter ; Wasserburger, Paul ; Golser, Robin: The ILIAMS project – An RFQ ion beam cooler for selective laser photodetachment at VERA. In: *Nuclear Instruments and Methods in Physics Research Section B: Beam Interactions with Materials and Atoms* 456 (2019),

213 - 217. http://dx.doi.org/https://doi.org/10.1016/j.nimb.2019.04.039. – DOI https://doi.org/10.1016/j.nimb.2019.04.039. – ISSN 0168–583X

[34] Martschini, Martin ; Pitters, Johanna ; Moreau, Tobias ; Andersson, Pontus ; Forstner, Oliver ; Hanstorp, Dag ; Lachner, Johannes ; Liu, Yuan ; Priller, Alfred ; Steier, Peter ; Golser, Robin: Selective laser photodetachment of intense atomic and molecular negative ion beams with the ILIAS RFQ ion beam cooler. In: *International Journal of Mass Spectrometry* 415 (2017), 9 - 17. http://www.sciencedirect.com/science/article/pii/S1387380616302378. – ISSN 1387–3806

[35] Pitters, Johanna: *Laser Photodetachment in a Gas-Filled RF-Quadrupole*, University of Vienna, Diplomarbeit, 2015

[36] Major, Fouad G. ; Gheorghe, Viorica N. ; Werth, Günther: *Charged Particle Traps*. 2005 https://link.springer.com/book/10.1007/b137836. – ISBN 9783540265764

[37] Paul, Wolfgang: Electromagnetic Traps for Charged and Neutral Particles (Nobel Lecture). In: *Angewandte Chemie International Edition in English* 29 (1990), Nr. 7, 739-748. https://onlinelibrary.wiley.com/doi/abs/10.1002/anie.199007391

[38] Mathieu Émile: Memoire sur le Mouvement Vibratoire d'une Membrane de Forme Elliptique. In: *Journal de Mathématiques Pures et Appliquées* 13 (1868), S. 137–203

[39] Shayeghi, Armin: personal communication.

[40] Rienstra-Kiracofe, Jonathan C. ; Tschumper, Gregory S. ; Schaefer, Henry F. ; Nandi, Sreela ; Ellison, G. B.: Atomic and Molecular Electron Affinities: Photoelectron Experiments and Theoretical Computations. In: *Chemical Reviews* 102 (2002), Nr. 1, 231-282. https://doi.org/10.1021/cr990044u

[41] Kasberger, Magdalena: *Accelerator Mass Spectrometry of Cesium Isotopes*, university of vienna, Diplomarbeit, 2015

[42] Kern, Michael: *Increased Negative Ionization Efficiency for the Detection of ^{236}U and ^{233}U by AMS*, University of Vienna, Diplomarbeit, 2020

[43] IFIN-HH: https://tandem.nipne.ro/9MV_Pelletron.php

[44] Petrunin, V. V. ; Voldstad, J. D. ; Balling, P. ; Kristensen, P. ; Andersen, T. ; Haugen, H. K.: Resonant Ionization Spectroscopy of Ba^-: Metastable and Stable Ions. In: *Phys. Rev. Lett.* 75 (1995), Sep, 1911–1914. https://link.aps.org/doi/10.1103/PhysRevLett.75.1911

[45] Eliades, J. ; Zhao, X.-L. ; Litherland, A.E. ; Kieser, W.E.: On-line ion chemistry for the AMS analysis of 90Sr and 135,137Cs. In: *Nuclear Instruments and Methods in Physics Research Section B: Beam Interactions with Materials and Atoms* 294 (2013), 361 - 363. http://www.sciencedirect.com/science/article/pii/S0168583X11010615. – ISSN 0168–583X

[46] Zhao, X.-L. ; Charles, C.R.J. ; Cornett, R.J. ; Kieser, W.E. ; MacDonald, C. ; Kazi, Z. ; St-Jean, N.: An exploratory study of recycled sputtering and $CsF2^-$ current enhancement for AMS. In: *Nuclear Instruments and Methods in Physics Research Section B: Beam Interactions with Materials and Atoms* 366 (2016), 96 - 103. http://www.sciencedirect.com/science/article/pii/S0168583X15010332. – ISSN 0168–583X

[47] MacDonald, C.M. ; Charles, C.R.J. ; Zhao, X.-L. ; Kieser, W.E. ; Cornett, R.J. ; Litherland, A.E.: Determination of 135Cs by accelerator mass spectrometry. In: *Nuclear Instruments and Methods in Physics Research Section B: Beam Interactions with Materials and Atoms* 361 (2015), 554 - 558. http://www.sciencedirect.com/science/article/pii/S0168583X15002086. – ISSN 0168–583X

[48] Martschini, Martin ; Lachner, Johannes ; Merchel, Silke ; Priller, Alfred ; Steier, Peter ; Wallner, Anton ; Wieser, Alexander ; Golser, Robin: The quest for AMS of ^{182}Hf - why poor gas gives pure beams (in revision). (2020)

[49] Lachner, Johannes: personal communication.

[50] MacDonald, Cole: *Measurement of radioactive caesium isotopes by accelerator mass spectrometry*, University of Ottawa, Diplomarbeit, 2014

[51] Bu, Wenting ; Ni, Youyi ; Steinhauser, Georg ; Zheng, Wang ; Zheng, Jian ; Furuta, Naoki: The role of mass spectrometry in radioactive contamination assessment after the Fukushima nuclear accident. In: *J. Anal. At. Spectrom.* 33 (2018), 519-546. http://dx.doi.org/10.1039/C7JA00401J

[52] Nuclear Data Center - Japan Atomic Energy Agency, Nuclide Information Sheet 136Cs. https://wwwndc.jaea.go.jp/cgi-bin/nuclinfo2014?55,136

[53] Nuclear Data Center - Japan Atomic Energy Agency, Nuclide Information Sheet 134Cs. https://wwwndc.jaea.go.jp/cgi-bin/nuclinfo2014?55,134

[54] Nagy, P. ; Vajda, N. ; Sziklai-László, I. ; Kovács-Széles, É. ; Simonits, A.: Determination of 135Cs in nuclear power plant wastes by ICP-MS and k0-NAA. In: *Journal of Radioanalytical and Nuclear Chemistry* 300 (2014), 5, 615-627. https://doi.org/10.1007/s10967-013-2875-2. – ISSN 2–1588–2780

[55] Alfa Aesar product specification 87640 cesium chloride. https://www.alfa.com/de/prodspec/087640

[56] Alfa Aesar product specification 11112 cesium sulfate. https://www.alfa.com/de/prodspec/011112

[57] Alfa Aesar product specification 12338 Barium fluoride. https://www.alfa.com/prodspec/012338

[58] Sigma Aldrich product specification Lead(II) Fluoride. https://www.sigmaaldrich.com/Graphics/COfAInfo/SigmaSAPQM/SPEC/23/236152/236152-BULK_____ALDRICH__.pdf

[59] Marek, Christoph: *AMS measurements of ^{36}Cl using isobar suppression via laser photodetachement*, University of Vienna, Diplomarbeit, 2018

[60] Lachner, Johannes ; Marek, Christoph ; Martschini, Martin ; Priller, Alfred ; Steier, Peter ; Golser, Robin: 36Cl in a new light: AMS measurements assisted by ion-laser interaction. In: *Nuclear Instruments and Methods in*

Physics Research Section B: Beam Interactions with Materials and Atoms 456 (2019), 163 - 168. http://www.sciencedirect.com/science/article/pii/S0168583X19303829. – ISSN 0168–583X

[61] The ETH Zurich AMS facilities: Performance parameters and reference materials. In: *Nuclear Instruments and Methods in Physics Research Section B: Beam Interactions with Materials and Atoms* 294 (2013), 29 - 38. http://www.sciencedirect.com/science/article/pii/S0168583X12001577. – ISSN 0168–583X

[62] Steier, Peter ; Martschini, Martin ; Buchriegler, Josef ; Feige, Jenny ; Lachner, Johannes ; Merchel, Silke ; Michlmayr, Leonard ; Priller, Alfred ; Rugel, Georg ; Schmidt, Edith ; Wallner, Anton ; Wild, Eva M. ; Golser, Robin: Comparison of methods for the detection of 10Be with AMS and a new approach based on a silicon nitride foil stack. In: *International Journal of Mass Spectrometry* 444 (2019), 116175. http://www.sciencedirect.com/science/article/pii/S1387380619301617. – ISSN 1387–3806

[63] Piacente, Vincenzo ; Brunetti, Bruno ; Scardala, Paolo: Thermodynamic Study of Sublimation of PbF2 and PbF4 from Torsion-Effusion Vapor Pressure Measurements. In: *Journal of Chemical & Engineering Data* 55 (2010), Nr. 9, 3731-3735. https://doi.org/10.1021/je100260z

[64] Alcock, C. B. ; Itkin, V. P. ; Horrigan, M. K.: Vapour Pressure Equations for the Metallic Elements: 298-2500K. In: *Canadian Metallurgical Quarterly* 23 (1984), Nr. 3, 309-313. https://doi.org/10.1179/cmq.1984.23.3.309

[65] Milota, Petra ; Reiche, Ina ; Duval, Alain ; Forstner, Oliver ; Guicharnaud, Hélène ; Kutschera, Walter ; Merchel, Silke ; Priller, Alfred ; Schreiner, Manfred ; Steier, Peter ; Thobois, Elisabeth ; Wallner, Anton ; Wünschek, Barbara ; Golser, Robin: PIXE measurements of Renaissance silverpoint drawings at VERA. In: *Nuclear Instruments and Methods in Physics Research Section B: Beam Interactions with Materials and Atoms* 266 (2008), Nr. 10, 2279 - 2285. http://www.sciencedirect.com/science/article/pii/S0168583X08002528. – ISSN 0168–583X

[66] Eisenhut, Christoph: *PIXE zur Entwicklung der Extraktionschemie für AMS Proben*, University of Vienna, Diplomarbeit, 2020

[67] Steier, Peter: personal communication.

[68] Snow, Mathew S. ; Snyder, Darin C. ; Mann, Nick R. ; White, Byron M.: Method for ultra-trace cesium isotope ratio measurements from environmental samples using thermal ionization mass spectrometry. In: *International Journal of Mass Spectrometry* 381-382 (2015), 17 - 24. http://www.sciencedirect.com/science/article/pii/S1387380615000986. – ISSN 1387–3806

[69] Snow, Mathew S. ; Snyder, Darin C.: 135Cs/137Cs isotopic composition of environmental samples across Europe: Environmental transport and source term emission applications. In: *Journal of Environmental Radioactivity* 151 (2016), 258 - 263. http://www.sciencedirect.com/science/article/pii/S0265931X15301417. – ISSN 0265–931X

[70] GESTIS Stoffdatenbank, GESTIS Material Database. https://www.dguv.de/ifa/gestis/gestis-stoffdatenbank/index.jsp

[71] Honda, Maki: personal communication.

[72] IAEA372 Reference Sheet. https://nucleus.iaea.org/rpst/Documents/rs_iaea_372.pdf

[73] Shakhashiro, A. ; Sansone, U. ; Arnold, D. ; Dryak, P. ; Rosa, Jerome J. L. ; Jerome, S.M. ; Makarewicz, M. ; Mentcheva, J. ; Sato, K. ; Tarjan, S.: The new IAEA-372 grass-certified reference material for 40K and 137Cs. In: *Applied Radiation and Isotopes* 66 (2008), Nr. 11, 1718 - 1721. http://www.sciencedirect.com/science/article/pii/S0969804308002522. – ISSN 0969–8043

[74] IAEA447 Reference Sheet. https://nucleus.iaea.org/rpst/Documents/RS_IAEA-447.final.pdf

[75] Shakhashiro, A. ; Tarjan, S. ; Ceccatelli, A. ; Kis-Benedek, G. ; Betti, M.: IAEA-447: A new certified reference material for environmental

radioactivity measurements. In: *Applied Radiation and Isotopes* 70 (2012), Nr. 8, 1632 - 1643. http://www.sciencedirect.com/science/article/pii/S0969804312002254. – ISSN 0969–8043